Improving response and reducing toxicity to immune checkpoint blockade therapy in melanoma

Hoefsmit, E.P.

4

Inhibitor of apoptosis proteins antagonist induces T-cell proliferation after cross-presentation by dendritic cells

E. P. Hoefsmit[1], P. T. van Royen[1], D. Rao[1], J. A. Stunnenberg[1], P. Dimitriadis[1], C. Lieftink[2], B. Morris[2], E. A. Rozeman[3], I. L. M. Reijers[3], R. Lacroix[1], H. Shehwana[1], M. A. Ligtenberg[1], R. L. Beijersbergen[2,4], D. S. Peeper* [1,4], C. U. Blank* [1,3,5]

* Corresponding authors

[1] Department of Molecular Oncology and Immunology, Netherlands Cancer Institute, Amsterdam, The Netherlands, [2] Robotics and Screening facility, Netherlands Cancer Institute, Amsterdam, The Netherlands, [3] Department of Medical Oncology, Netherlands Cancer Institute, Amsterdam, The Netherlands, [4] Oncode Institute, The Netherlands, [5] Department of Internal Medicine, Leiden University Medical Center, Leiden, The Netherlands

Cancer Immunology Research, 2023, 11.4: 450-465.
doi: 0.1158/2326-6066.CIR-22-0494

Abstract

Cross-presentation of tumor antigens by dendritic cells (DC) is crucial to prime, stimulate and restimulate $CD8^+$ T cells. This process is important in initiating and maintaining an antitumor response. Here, we show that the presence of conventional type 1 DCs (cDC1), a DC subtype that excels in cross-presentation, in the tumor correlated with response to neoadjuvant immune checkpoint blockade (ICB) in melanoma. This led us to hypothesize that patients failing to respond to ICB could benefit from enhanced cross-presentation of tumor antigens. We therefore established a cross-presentation assay to screen over 5,500 compounds for enhancers of DC cross-presentation using induced T-cell proliferation as the readout. We identified 145 enhancers, including AZD5582, an antagonist of inhibitor of apoptosis proteins (IAP) cIAP1, cIAP2, and XIAP. AZD5582 treatment led to DC activation of the noncanonical NF-kB pathway, enhanced antigen import from endolysosomes into the cytosol, and increased expression of genes involved in cross-presentation. Furthermore, it upregulated expression of CD80, CD86, MHC class II, CD70 and secretion of TNF by DCs. This enhanced DC activation and maturation program was observed also in tumor-bearing mice upon AZD5582 treatment, culminating in an increased frequency of systemic tumor antigen–specific CD8. T cells. Our results merit further exploration of AZD5582 to increase antigen cross-presentation for improving the clinical benefit of ICB in patients who are unlikely to respond to ICB.

Introduction

Immune checkpoint blockade (ICB) therapy has resulted in substantial clinical benefit in a subset of cancers (1). In late stage melanoma, ICB is currently one of the most effective standard therapies (2-6), showing a 55% overall survival at 7.5 years for patients treated with the combination of nivolumab (anti-programmed cell death 1; anti-PD-1) and ipilimumab (anti-cytotoxic T-lymphocyte protein 4; anti-CTLA-4) (5, 7). High response rates (70-80%) are observed particularly in the neoadjuvant setting (8-10) and are associated with long-term relapse free survival (RFS; 2-year 96%) (10). Despite the success of ICB therapy, a substantial group of patients fail to durably respond. Hence, there is a need for a better understanding of the mechanisms and rate-limiting steps involved in ICB therapy response and for the development of new approaches to increase it.

The efficacy of ICB therapy largely depends on tumor antigen-specific $CD8^+$ T cells in the tumor microenvironment (TME) (11). Priming, re-stimulation and expansion of tumor-specific $CD8^+$ T cells require cross-presentation of tumor-associated antigens by dendritic cells (DCs). This involves uptake of exogenous tumor cell fragments followed by tumor antigen processing, Major Histocompatibility Complex (MHC) class I loading and presentation on the cell surface (12). Especially the specialized conventional type I DCs (cDC1s, also called "Batf3-dependent" DCs) excel in (tumor) antigen cross-presentation. In recent years, the importance of cDC1s has been highlighted by pre-clinical data, demonstrating that rejection of immunogenic tumors and response to ICB requires cross-presenting cDC1s (13-20). This is consistent with clinical studies showing an association between abundance of cDC1s in tumors with increased survival and response upon ICB therapy (21, 22). However, cDC1s are rare within the TME and are often excluded from tumors (14, 21).

Therefore, therapies that increase antigen cross-presentation might provide new ways to restore anti-tumor immunity and overcome resistance to ICB. Different promising approaches have been explored, for example, to enhance DC maturation (e.g., by a Toll-like receptor 9 (TLR9) or TLR3 agonist, FLT3L, XCL1) (16, 23-26), to improve antigen delivery by antibody-antigen conjugates (e.g., DEC-205, Clec9A/DNGR1) (27-29), or to promote antigen presentation by DCs with a neoantigen vaccine (30). However, these different approaches have a few drawbacks, since an accessible tumor lesion is required for intratumor administration of the agent(s), or because they are expensive to implement due to the requirement for prior identification of neoantigens for every individual patient.

This prompted us to develop an alternative strategy for enhancing $CD8^+$ T cell priming by DCs. We established a cross-presentation assay to screen over 5,500 compounds to

identify novel therapeutic compounds that improve $CD8^+$ T proliferation after cross-presentation of tumor-associated antigens by bone marrow-derived DCs (BMDCs).

Methods

Patient samples

In the phase 2 OpACIN-neo trial and PRADO extension cohort (NCT002977052) (31, 32), 185 treatment naïve patients (n=86 OpACIN-neo, n=99 PRADO) with macroscopic stage III melanoma were treated with combination neoadjuvant therapy of anti-CTLA-4 (ipilimumab) and anti-PD-1 (nivolumab). All study details (trial designs, eligibility criteria, assessment) have been reported previously (9, 31, 32). The studies were conducted in accordance with Good Clinical Practice guidelines as defined by the International Conference of Harmonization and the Declaration of Helsinki. Pre-treatment tumor biopsies were taken for all patients. RNA (n=144) and DNA (n=64, only OpACIN-neo trial) were extracted from biopsies that had sufficient tumor material based on pathologist's scoring, respectively for RNA and DNA sequencing analysis, as reported previously (31). The libraries from patient samples of the PRADO study were sequenced on NovaSeq6000 (Illumina Inc.) at CeGaT (Tuebingen, Germany). FASTQ files were mapped to human reference genome (Homo.sapiens.GRCh38.v101) using STAR(2.7.3a) (33), count data was generated with HTseq-count (version 0.12.4) (34), ensemble gene ID and mgi symbol linkage was obtained using biomart (version 2.46.3) (35) and analyzed with DESeq2 (version 1.30.1) (36). The previously defined Batf3 DC-associated RNA gene signature (18), microenvironment cell population (MCP counter) (37) and Danaher immune cell signature (38) were analyzed on normalized gene expression data.

For whole-exome sequencing analysis, quality of the FASTQ files was analyzed with FastQC (version 0.11.5-cegat) and multiQC (version 1.12). FASTQ files were aligned to the human reference genome (GRCh38) using Burrows-Wheeler aligner (version 0.7.12) (39), as reported previously (31). Base quality scores were recalibrated using BaseRecalibrator in GATK (version 4.0.6.0), and single-nucleotide variants were called and filtered using MuTect2 in GATK (version 4.2.5.0) (40). The tumor mutational burden (TMB) was calculated by summarizing the total number of nonsynonymous, somatic mutations per sample with minimal variant allele frequency of 0.05 (5%). In addition, cross-sample contamination was analyzed using GATK CalculateContamination tool. Correct matching between normal and tumor pairs was analyzed using BAMixChecker phyton tool (version 1.0).

Mice

C57BL/6JRj were obtained from Janvier. Cas9-EGFP mice and OT-I mice (OT-I TCR) were purchased from Jackson Laboratory. OT-1/Cas9 mice (OT-I mice crossed with Cas9-EGFP

mice, Jackson Laboratory) were generated in the animal facility of the Netherlands Cancer Institute (41). Animals were maintained under standard housing conditions. Mice in the *in vivo* antigen presentation and tumor model experiments were given, in addition to *ad libitum* access to drinking water and chow food, also nutritionally fortified water gel (DietGel Recovery; ClearH2O). All animal procedures (organ harvesting and *in vivo* experiments) were approved by the Animal Welfare Committee of the Netherlands Cancer Institute, in accordance with institutional and national guidelines.

Cell lines

The murine melanoma B16F10 cell line was previously obtained from ATCC, which was used for this study from 2018 onwards. The B16F10-OVA cell line was generated by transduction with a lentiviral construct encoding for full-length cytoplasmic ovalbumin protein (42), and was under the continuous selection control of hygromycin B (Invitrogen, 10687010). To generate B16F10 and B16F10-OVA β2-Microglobulin-deficient ($\beta2M^{-/-}$) cell lines ($B16F10^{B2m-/-}$ and $B16F10\text{-}OVA^{B2m-/-}$), tumor cells were transduced with lentiCRISPR-v2 targeting murine β2M and sorted by flow cytometry based on absence of $H\text{-}2K^{b}$ expression after stimulation with 100 ng/ml interferon gamma (IFN-γ) for 24 hours (43). The murine colorectal cell line MC38 used for experiment was from the Peeper lab cell stock (2021). Cell lines were cultured in DMEM (Gibco, 41966) supplemented with 10% heat-inactivated fetal bovine serum (FBS; Capricorn Scientific, 3101517) and 1% penicillin/streptomycin (P/S; Gibco, 15140130). Cell lines were kept in culture for 3-4 weeks. All cell lines were routinely confirmed to be mycoplasma-negative and not re-authenticated.

BMDCs culture

Bone marrow (BM) cells were harvested by flushing the femurs and tibia from both hind legs of Cas9-EGFP or WT C57BL/6JRj mice. Erythrocyte-lysed BM cells were directly used for BMDC differentiation (44) and cultured in DC culture media, containing RPMI 1640 (Thermo Fisher, 11875093), 10% heat-inactivated FBS, 1% P/S, 2 mM L-glutamine (Thermo Fisher, 255030081), 10 mM HEPES buffer (Thermo Fisher, 15630080), 1 mM sodium-pyruvate (Thermo Fisher, 11360070), 1% MEM non-essential amino acids (Thermo Fisher, 1140035) and 50 μM β-mercaptoethanol (Merck, 444203).

GM-CSF DCs

For the generation of granulocyte-macrophage colony stimulating factor (GM-CSF) DCs, BM cells were cultured in the presence of GM-CSF. 2×10^{6} BM cells were plated in a 100mm sterile Petri dishes (SarsTedt) in the presence of DC culture media (10 mL) supplemented with 20 ng/ml GM-CSF (Immunotools, 12343125). After three days, DC culture media (10 mL) containing 20 ng/ml GM-CSF was added. On day 6, half of the

medium was refreshed with new DC culture media containing 20 ng/ml GM-CSF. GM-CSF DCs were used on day 9 for subsequent experiments, unless stated otherwise.

GM-CSF + FLT3L DCs

GM-CSF + FMS-Like Tyrosine Kinase 3 Ligand (FLT3L) DCs were generated from BM cells, 10-15 x 10^6 cells were plated in 100mm sterile Petri dishes in the presence of DC culture media (10 mL) supplemented with 20 ng/ml GM-CSF and 200 ng/ml FLT3L (Fisher Scientific, 11554970). After six days, DC culture media (10 mL) was added. On day 9, cells were harvested and 3 x 10^6 cells were replated in DC culture media (10 mL) supplemented with 20 ng/ml GM-CSF and 200 ng/ml FLT3L. GM-CSF + FLT3L DCs were used on day 16 for subsequent experiments.

Pan DC culture

Pan DCs (both classical DCs and plasmacytoid DCs) were isolated from spleens from Cas9-EGFP or WT C57BL/6JRj mice using Pan Dendritic Cell Isolation Kit (Miltenyi Biotec, 130-100-875). Briefly, spleens were mashed through a 70-µm filter (BD Biosciences) and incubated in erylysis buffer (Biolegend, 420301) on ice for 7 minutes. Next, cells were counted and isolated following manufacturer's instructions. The unbound fraction, containing the Pan DCs, were resuspended in DC culture media and used for subsequent experiments. Pan-DCs were seeded at 0.4-0.5 x 10^6 cells/mL in a non-tissue-culture treated 24-well plate (Corning) and treated with 0.5 µM AZD5582 (MedChemExpress, HY-12600) or corresponding volume of DMSO (Sigma-Aldrich, 34943-1L-M). After 24 hours of treatments, cells were harvested, either stained for marker analysis (as described in flow cytometry analysis) or used to analyze cytosolic import of antigens (as described in cytosolic import analysis).

$CD8^+$ T cells

Spleens of OT-I TCR or OT-I/Cas9 mice were harvested and single cell suspension was obtained by mashing spleens through a 70-µm filter. Subsequently, cells were resuspended in erylysis buffer. The cells were counted and $CD8^+$ T cells were isolated using $CD8a^+$ T cell isolation kit (Miltenyi Biotec, 130-104-075) following manufacturer's instructions. The unlabeled fraction, containing the $CD8^+$ T cells, were collected and labelled with CellTrace™Violet (CTV) Cell Proliferation Kit (Thermo Fisher, C34557) according to manufacturer's instructions. CTV-labelled $CD8^+$ T cells were directly used in the subsequent experiments as described.

Cross-presentation assay

For cross-presentation of cell-associated antigens, DCs (GM-CSF DCs or GM-CSF + FLT3L DCs) were incubated in the presence of irradiated B16F10-OVA$^{B2m-/-}$ cells, naïve CTV-labelled OT-I TCR specific $CD8^+$ T cells and 1 µM of CpG oligodeoxynucleotide (ODN)

class B (Invivogen, Tlrl-1826-5) in a sterile V-bottom 384-well plate (Greiner, cat no. 781281) at 1:1:1 ratio (10,000 cells each cell type) in DC culture media. B16F10-OVA$^{B2m-/-}$ cells were irradiated with 100 Gray (Gy) using a Gammacell 40 Extractor (Theratronics). DCs, B16F10-OVA$^{B2m-/-}$, CD8$^+$ T cells and CpG ODN class B were added by hand or using the Multidrop^{TM} Combi Reagent Dispenser (Thermo Scientific). For cross-presentation assays in the presence of compounds, the HP D300 Digital Dispenser (Tecan) was used to dispense compounds at indicated dose (Table 1). After four days of incubation at 37˚C, cells were washed, stained and measured with flow cytometry.

For pre-treatment, GM-CSF DCs were treated with AZD5582 prior to the cross-presentation assay. First, 0.5 x 10^6 GM-CSF DCs were harvested on day 8 of differentiation protocol and treated with AZD5582 (0.1 μM – 1 μM) or corresponding volume of DMSO control in DC culture media in a non-tissue-culture treated 24-well plate. After 24 hours of incubation at 37˚C, cells were washed two times, counted and replated at 10,000 cells, together with irradiated B16F10-OVA$^{B2m-/-}$, naïve CTV-labelled OT-I TCR specific CD8$^+$ T cells and 1 μM of CpG ODN class B, as described in cross-presentation assay, without the presence of AZD5582. After four days of culture at 37˚C, cells were washed, stained and measured with flow cytometry.

To assess the effect of AZD5582 on T cells, a cross-presentation assay was performed as described earlier, without the presence of DCs. Naïve CTV-labelled OT-I TCR specific CD8$^+$ T cells were cultured in the presence of irradiated B16F10-OVA$^{B2m-/-}$, 1 μM CpG ODN class B with the addition of AZD5582 at a dose range (0.05 μM – 5 μM). In addition, plates were pre-coated with anti-CD3 (0.5 μg/mL, eBiosciences) and anti-CD28 (5 μg/mL, eBiosciences) antibodies. To these plates, naïve CTV-labelled OT-I TCR specific CD8$^+$ T cells, irradiated B16F10-OVA$^{B2m-/-}$, 1 μM CpG ODN class B and AZD5582 at a dose range (0.05 μM – 5 μM) was added. After four days of incubation at 37˚C, cells were washed, stained and measured with flow cytometry.

Compound Screen

The Oncode Repurposing Drug Library (45) was used to screen for compounds that enhance T cell proliferation after cross-presentation of tumor antigens by GM-CSF DCs. The same setting of the cross-presentation assay was applied, using GM-CSF DCs (and B16F10-OVA$^{B2m-/-}$ tumor cells, naïve CTV-labelled OT-I TCR specific CD8$^+$ T and CpG ODN class B) in the presence of DMSO (instead of a compound) as negative control and GM-CSF + FLT3L DCs (instead of GM-CSF DCs) in the presence of DMSO as positive control. The positive and negative controls were included on every screen plate. A total of 5632 different compounds were screened, at a dose of 0.5 μM. All compounds were screened in three technical replicates, using three identical independent plates. The 384-well plates (total of 63) were incubated for four days at 37˚C. Next, supernatant

was saved, cells were washed, stained and CTV was measured using the Intellicyt® iQue™ to determine the number of proliferated $CD8^+$ T cells. To assess the performance of the iQue Screener, Rainbow Calibration Particles (8 peaks; Biolegend, 422903) were included on every plate.

Normalization of the number of proliferated $CD8^+$ T cells was done by subtracting the median of all wells with a compound well. Quality control was based on Z-factor (46) caluculation, assessing how well positive controls can be separated from negative controls. Plates with a Z-factor lower than 0 were excluded from the analysis. In addition, the correlation between three plate replicates was determined. Plate replicates were removed when the correlation R^2 between the other two replicates was more than 1.5 times the mean R^2 of this specific plate replicate and the other two replicates. Hits were detected using the strictly standardized mean difference (SSMD) = $\frac{\mu 1-\mu 2}{\sqrt{\sigma 1^2+\sigma 2^2}}$, where μ_1 corresponds to mean of experimental well, μ_2 corresponds to mean of negative control and σ_1 and σ_2 the SDs of the corresponding populations (47). A cut-off of SSMD ≥ 3 was used for hit detection.

Cytokine analysis

Cytokine concentration in the supernatant of different experiments were analyzed by cytometric bead array (CBA; BD Biosciences). The supernatant at the end of cross-presentation assay (after four days, as described before) was collected and stored at -20°C. The supernatant of GM-CSF DCs and GM-CSF + FLT3L DCs cultured in the presence of AZD5582 for 24 hours was also collected and stored at -20°C. Supernatant was thawed on ice and the concentrations of IFN-γ (558296), tumor necrosis factor (TNF, 558299), interleukin-2 (IL-2, 558297) and IL-12p70 (558303) were analyzed by CBA according to the manufacturer's instructions.

Flow cytometry analysis

Cells were stained at the end of a cross-presentation assay for flow cytometry analysis, as earlier described. After removal of supernatant, cells were washed with FACS buffer, consisting of 0.5% Bovine Serum Albumin (BSA, 10735094001) and 2mM ethylenediaminetetraacetic acid (EDTA; Lonza, LO 51201) in PBS. For other flow cytometry analysis, DCs (GM-CSF DCs, GM-CSF + FLT3L DCs, Pan DCs, human monocyte derived DCs (moDCs)) were incubated with different concentrations of AZD5582 and harvested after 24 hours. Supernatant was removed and cells were washed with FACS buffer. Single cell suspensions from tumor, spleen, lymph nodes and blood were obtained as described in *in vivo* experiments. Next, cells were Fc-blocked using CD16/CD32 antibody (Thermo Fisher, 14-0161-85) and subsequently stained with fluorochrome conjugated antibodies (Table 1). After incubation, samples were washed in FACS buffer and analyzed on

Intellicyt® iQue™ or LSR Fortessa (BD Biosciences) and data was analyzed using FlowJo Software (Treestar Inc. v10).

Cytosolic import assay

For the cytosolic assay the antigen import into the cytosol of either GM-CSF DCs or Pan-DCs was tested. GM-CSF DCs harvested on day 8 of the differentiation protocol and isolated Pan-DCs were treated in a non-tissue-culture treated 24-well plate with 0.5 μM AZD5582 or corresponding volume of DMSO in DC culture media for 24 hours. Next, the cells were washed and seeded at 1,500,000 cells/well for GM-CSF DCs and 50,000 cells/well for Pan-DCs in a U-bottom 96-well plate (Greiner) and incubated with 10 mg/mL β-lactamase (penicillinase; Sigma-Aldrich, P0389) in DC culture media. After three hours of incubation at 37˚C, cells were washed with PBS and loaded with CCF4 using the LiveBlazer-FRET B/G Loading Kit (Thermo Fisher, K1095) following the manufacturer's instructions and incubated for 30 minutes at room temperature protected from light. Next, the cells were washed, Fc-blocked using CD16/CD32 antibody and stained with LIVE/DEAD™ near-IR Dead Cell Stain Kit (Thermo Fisher, L34976) and indicated fluorochrome conjugate antibodies (Table 1), diluted in PBS with 0.5% BSA and 2 mM EDTA. Subsequently, samples were analyzed on LSR Fortessa. The fraction of live cells with a high expression of V450 fluorescence were used as a measure for efficient antigen import into the cytosol.

Sequencing

GM-CSF DCs on day 8 of the differentiation protocol and GM-CSF + FLT3L DCs on day 16 were harvested. In addition, GM-CSF DCs or GM-CSF + FLT3L DCs were treated with AZD5582 or the same volume of DMSO for 24 hours. DCs were harvested, washed and cell pellets were snap-frozen. RNA isolation and sequencing was performed by CeGaT. Briefly, total RNA was isolated using RNeasy Mini Kit (Qiagen, 740104). Quantity of RNA was measured by Qubit (Thermo Fisher) and quality profile was made using the Fragment analyzer (Agilent). Total RNA samples having RIN>8 were subjected to library generation. The library was prepared using TruSeq Stranded mRNA kit (Illumina, 20020594) according to the manual and analyzed using the Fragment analyzer. The libraries were sequenced on NovaSeq6000 (Illumina Inc.). The samples were mapped with STAR (version 2.7.3a) to mouse reference genome Mus_musculus.GRCm39.105 or to human reference genome Homo_sapiens.GRCh38 using default settings (33). The read counts were computed with HTseq-count (version 0.12.4) and were analyzed with DESeq2 (DESeq2_1.30.1) (34). Centering of the normalized gene expression read counts was performed by subtracting the row means and scaling by dividing the columns by the standard deviation (SD) to generate a z-score.

Immunoblot analyses

GM-CSF DCs were treated with AZD5582 or similar volume of DMSO for indicated time points (2–24 hours). Next, GM-CSF DCs were harvested, washed with PBS and lysed in RIPA buffer (50 mM TRIS pH 8.0, 150 mM NaCl, 1% NP40, 0.5% sodium deoxycholate, 0.1% SDS) with Halt™ Protease and Phosphatase Inhibitor Cocktail (Thermo Fisher, 78444) for 30 minutes on ice. Next, protein concentration was measured by Bradford Protein Assay (Biorad, 5000006). Samples were run on 4%–12% Bis-Tris polyacrylamide-SDS gels (Thermo Fisher) and transferred on to nitrocellulose membranes (GE Healthcare) using the iBlot system (Thermo Fisher). Ponceau S (Merck) was used to assess protein loading and transfer. The membranes were incubated in blocking buffer (4% BSA, 0.2% Tween-20 in PBS) for one hour. For NF-kB–inducing kinase (NIK), blocking was performed using either 4% Elk-milk (Campina) or 4% BSA. Next, membranes were incubated with primary antibodies (diluted 1:1000 in blocking buffer) overnight, followed by washing three times with washing buffer (0.2% Tween-20 in PBS) for 5 minutes each. After washing, the membranes were incubated with secondary antibody (diluted 1:5,000 in blocking buffer) for 1 hour, followed by washing three times as described before. Next, membranes were exposed to Clarity™ Western ECL substrate (Bio-rad, 1705061) or SuperSignal™ West Dura Extended Duration Substrate (Thermo Fisher, 34075) and visualized using ChemiDoc™ Imaging System (Bio-Rad). Protein bands were analyzed and quantified using FIJI ImageJ (v2.0.0). Primary antibodies against mouse cellular inhibitor of apoptosis protein-2 (cIAP-2; R&D systems), cIAP-1 (abcam), X-linked inhibitor of apoptosis protein (XIAP), NIK, p100/-52, cyclophilin b, β-actin (all from Cell Signaling) and HSP90 (BD Biosciences) were used (**Table 1**). Horseradish peroxidase (HRP)-conjugated secondary antibodies against mouse or rabbit were used (Thermo Fisher).

Human DC generation

Human moDCs were generated from healthy donor buffy coats, as described by Ali et al. (48). In brief, buffy coats from healthy donors were obtained from Sanquin Amsterdam. Next, peripheral blood mononuclear cells (PBMCs) were isolated through Ficoll (Fisher Scientific) gradient separation and cells were stored at -80 °C. After thawing, monocytes were isolated with positive bead labeling using CD14 MicroBeads (Miltenyi Biotec, 130-050-201) following the manufacturer's instructions. Isolated $CD14^+$ cells were resuspended at 1 x 10^6 cells/ml in DC medium (GMP DC medium (CellGenix®, 20801-0500) supplemented with 1% human serum (Sigma-Aldrich, H3667) and 1% P/S) with the addition of 50 IU/ml human recombinant IL-4 (Peprotech, 200-04) and 800 IU/ml human recombinant GM-CSF (Peprotech, 300-03) in a six-well plate (Corning). After 48 hours, DC medium with 200 IU/ml IL-4 and 3200 IU/ml GM-CSF was added and the cells incubated for an additional 24 hours at 37°C. The next day, more DC medium was added with 50 IU/ml IL-4 and 800 IU/ml GM-CSF, in the presence of 0.5 μM AZD5582 or corresponding volume of control. After 24 hours, adherend DCs were dislodged from

the plate and used for flow cytometry analysis or snap-frozen and stored at -80 °C as cell pellets for subsequent RNA sequencing.

In vivo tumor experiments

0.5 x 10^6 B16F10-OVA cells or MC38 cells were resuspended in 50 µl of PBS and 50 µl of Matrigel (Corning, 734-1100) and subcutaneously (s.c.) injected in the right flank of 9-week-old female C57BL/6JRj mice. Tumor growth was followed three times weekly by caliper measurements of the greatest longitudinal diameter (length) and greatest transverse diameter (width), and tumor volume was calculated by the modified ellipsoidal formula: Tumor volume = length (mm) x width (mm) x (width (mm)/2). Mice were randomized into different treatment arms based on tumor volume and treatment was started at day 7 for B16F10-OVA and day 8 for MC38. AZD5582 (dissolved in DMSO: CremphorEL: water (1:1:8) at dose 0.5 mg/kg), anti–PD-1 (100 µg/mouse, clone: RMP1-14, BioXcell), anti–CTLA-4 (50 µg/mouse, clone: 9D9, BioXcell) or corresponding isotype controls (BioXcell, clone: 2A3 and clone: MPC-11) were injected and treatment lasted for a period of two weeks.

For B16F10-OVA, tumors, draining lymph node and spleens of satellite mice of the different treatment groups were harvested after 5 days of treatment. Single cell suspensions from tumors were obtained by mechanical disruption of the tissue by slicing followed by enzymatic digestion in medium containing 2 mg/ml collagenase A (Roche, 11088793001) and 1 mg/ml DNAse (Sigma-Aldrich, 4716728001) for 1 hour at 37 °C. The suspension was filtered through a 70-µm filter to remove debris. Single cell suspensions of lymph nodes and spleens were obtained by homogenizing the tissue through a 70-µm filter and spleens were incubated with erylysis buffer on ice for five minutes. These single cell suspensions were analyzed for T-cell activation and DC activation by flow cytometry.

Tumor growth was followed in the rest of the mice from the different treatment groups. Mice were euthanized by CO_2 asphyxiation when the predetermined experimental endpoint (tumor volume exceeded average 1,500 mm^3) was reached or when tumors bled and ulcerated or caused significant discomfort. The tumor sizes were plotted as tumor volume and compared to each treatment group as long as all mice did not exceed tumor volume endpoint.

In vivo vaccination experiment

C57BL/6JRj mice were injected intravenous (i.v.) with 0.7 x 10^6 CTV-labeled naïve OT-I $CD8^+$ T cells in 200 µl of PBS (as described in $CD8^+$ T cells). The next day, mice were injected (i.v.) with irradiated (100Gy) 0.4 x 10^6 B16F10-OVA$^{B2m-/-}$ cells or irradiated (100Gy) 0.4 x 10^6 B16F10$^{B2m-/-}$ cells and 25 µg CpG ODN Class B in 200 µl of PBS. In addition, mice

were either injected (i.p.) with 0.5 mg/kg AZD5582 (dissolved in DMSO: CremphorEL: water (1:1:8)) or vehicle control (DMSO: CremphorEL: water (1:1:8)). On day 5, lymph nodes and blood were isolated. Single cell suspension of lymph nodes was obtained by homogenizing the tissue through a 70-µm filter. Blood samples were incubated twice with erylysis buffer on ice for five minutes. These single cell suspensions were analyzed for T cell proliferation and DC activation by flow cytometry.

In mice that were challenged with B16F10-OVA tumors, mice were injected i.v. with 1 x 10^6 CTV-labeled naïve OT-I $CD8^+$ T cells in 200 µl of PBS (as described in $CD8^+$ T cells). The next day, mice were injected (i.v.) with irradiated (100Gy) 0.4 x 10^6 B16F10-$OVA^{B2m-/-}$ cells and 25 µg CpG ODN Class B in 200 µl of PBS. In addition, mice were either injected (i.p.) with 0.5 mg/kg AZD5582 (dissolved in DMSO: CremphorEL: water (1:1:8)) or vehicle control (DMSO: CremphorEL: water (1:1:8)). On day 3, mice were s.c. injected with 10,000, 100,000 or 1,000,000 B16F10-OVA cells resuspended in 50 µl of PBS and 50 µl of Matrigel. Tumor growth was followed in the mice from the different treatment groups.

Quantification and statistical analysis

All graphic visuals and statistical analysis were performed using Prism (Graphpad Software Inc., version 9) or in R (version 4.0.4) and R studio (version 1.4.1106) using the packages survminer (version 0.4.9), ggplot2 (version 3.3.5), cutpointr (version 1.1.2), heatmap3 (version 1.1.9), ROCit (version 2.1.1) and RColorBrewer (version1.1.-3)

The summary receiver operating characteristic (sROC) curves were computed based on the TMB or Batf3-DC score (average expression Batf3 DC-associated (*BATF3, CLEC9A*, *IRF8*, *THBD*, *XCR1*)) (18) between patients with and without a pathologic response. Optimal cutoffs were computed using the cutpointr package in R.

Two-tailed Student's t test was used to compare two means. Mean values of multiple groups to one control were compared using a one-way ANOVA followed by Dunnett's test to correct for multiple comparisons. *In vivo* data were compared by using multiple unpaired two-tailed Student's t test. Survival analysis was performed by Log-Rank Mantel-Cox test. Additional information about quantification and statistical analyses performed are described in the corresponding figure legends. P value lower than 0.05 was regarded statistically significant. *, $P<0.05$, **, $P<0.01$, ***, $P<0.001$, ****, $P<0.0001$.

Data availability

The DNA-sequencing and RNA-sequencing data of the OpACIN-neo study is available on reasonable request via the European Genome-phenome Archive (EGA) under the accession codes EGAS00001004832 (DNA) and EGAS00001004833 (RNA). Data requests will be reviewed by the institutional review board of the Netherlands Cancer Institute

and applying researchers will need to sign a data access agreement after approval. The sequencing data discussed in this publication have been deposited in NCBI's GENE Expression Omnibus (49) and are accessible through GEO Series accession number GSE217048 and GSE217050.

Results

Batf3-DC score is associated with response to neoadjuvant ICB

To assess the importance of Batf3-dependent DCs (cDC1s) in the setting of neoadjuvant ICB treatment, we determined whether its gene expression profile was associated with response in a large cohort of melanoma patients. In this cohort, patients with macroscopic stage III melanoma were treated with neoadjuvant treatment of anti-CTLA-4 (ipilimumab) plus anti-PD-1 (nivolumab) in two cohorts of our phase 2 trial (OpACIN-neo and PRADO; NCT02977052) (9, 31, 50). To determine the presence of cross-presenting DCs, we analyzed the baseline lymph node tumor biopsies for the expression of the Batf3 DC-associated genes (*BATF3, CLEC9A*, *IRF8*, *THBD*, *XCR1*) (18) (**Figure 1A**) and calculated their average expression (Batf3-DC score). A significantly higher expression profile was observed for patients with pathological response compared to patients without (*P*=0.0019; **Figure 1B**).

Previously, we have shown that patients achieving a pathological response to neoadjuvant ICB treatment had a higher TMB compared to non-responders (31). Since both the Batf3-DC score and TMB were significantly associated with pathologic response, we assessed whether these parameters were independent variables. No correlation between Batf3-DC score and TMB was observed (R=0.023; *P*=0.25; **Figure S1A**). Subsequently, we evaluated whether we were able to further identify non-responder patients based on their TMB and Batf3-DC score, using the sROC curves for defining the optimal cut-off (**Figure S1B**). Using this strategy, we observed that patients with either a high TMB/low Batf3-DC score (n=28), low TMB/high Batf3-DC score (n=7) or high TMB/high Batf3-DC score (n=16) had relatively high response rates (75%, 71% and 94% respectively; **Figure 1C**). In contrast, of the patients with a low TMB/low Batf3-DC score (n=8), only 13% showed a pathological response. A proportion of the non-responder patients still showed a relatively high expression of infiltration of other mononuclear phagocytes (**Figure S1C**). Only 38% of the patients with this double-low score achieved 2-year event-free survival (EFS) compared to 64-88% of the patients in the other three groups (*P*=0.016; **Figure 1D**). Thus, using our combined strategy, we identified a subgroup of patients that may benefit from additional therapies, including strategies to improve T cell priming by cross-presentation of tumor antigens by DCs.

Compound screen identifies for enhancers of T cell proliferation cross-presentation by DCs

Tumor antigen cross-presentation by DCs is a crucial step to mount an effective $CD8^+$ T cell response against the tumor (51). This prompted us to develop a screening model to identify compounds that improve T cell proliferation after cross-presentation of tumor antigens by DCs. We first optimized a cross-presentation assay, using murine bone marrow cells that were cultured in the presence of either GM-CSF alone (GM-CSF DCs) or supplemented with FLT3L (GM-CSF + FLT3L DCs). The latter correspond to Batf3-dependent DCs (44) and served as a positive control. Next, these GM-CSF DCs or GM-CSF + FLT3L DCs were incubated with irradiated B16F10-$OVA^{B2m-/-}$ tumor cells, CpG ODN class B and naïve CTV-labelled $CD8^+$ T cells that have a TCR specificity for $OVA_{257-264}$ (SIINFEKL) in the context of H-$2k^b$ (OT-I TCR) (52). The addition of TLR9 agonist CpG ODN class B was necessary for GM-CSF + FLT3L DCs to induce $CD8^+$ T cell proliferation in this cross-presentation assay. The engineered loss of $ß_2$ microglobulin (B2m) expression by the B16F10-OVA tumor cells ensured that no direct antigen-specific activation of the T cells by the tumor cells could occur (**Figure S2A**). Thus, in this setting, only tumor antigens (OVA) that have been processed into the SIINFEKL peptide and are presented in the context of H-$2k^b$ by the DCs can induce $CD8^+$ T cell proliferation and activation.

After four days, a sharp induction of $CD8^+$ T cell proliferation was observed when $CD8^+$ T cells and B16F10-$OVA^{B2m-/-}$ tumor cells were cultured in the presence of GM-CSF + FLT3L DCs, whereas cross-presentation of tumor antigens by GM-CSF DCs were less capable of inducing $CD8^+$ T cell proliferation (**Figure S2B, C**). This low induction of T cell proliferation by GM-CSF DCs formed the basis of the screen, because it was associated with a window to improve the induction of T cell proliferation after cross-presentation of tumor antigens by DCs.

To identify compounds improving this process of cross-presentation, we performed a screen with the Oncode Drug Library (over 5,500 compounds) using GM-CSF DCs incubated with irradiated B16F10-$OVA^{B2m-/-}$ tumor cells, CpG ODN class B and CTV-labeled naïve OT-I $CD8^+$ T cells (**Figure 2A**). After four days, CTV dilution of $CD8^+$ T cells was assessed by flow cytometry. For screen set-up controls, GM-CSF DCs (negative control) or GM-CSF + FLT3L DCs (positive control) were treated with the same volume of DMSO and included on each plate to track technical quality. Cross-presentation of tumor antigens by GM-CSF + FLT3L caused effective $CD8^+$ T cell proliferation, whereas almost no $CD8^+$ T cell proliferation was observed when GM-CSF DCs were used. This was consistently observed across all plates, highlighting the quality of the screen (**Figure 2B**, **Figure S3A-C**). In addition, the concentration of the proinflammatory cytokine IFN-γ was determined in the supernatant, where higher levels were observed when GM-CSF + FLT3L DCs were used in the cultures (**Figure 2C**, **Figure S2D**).

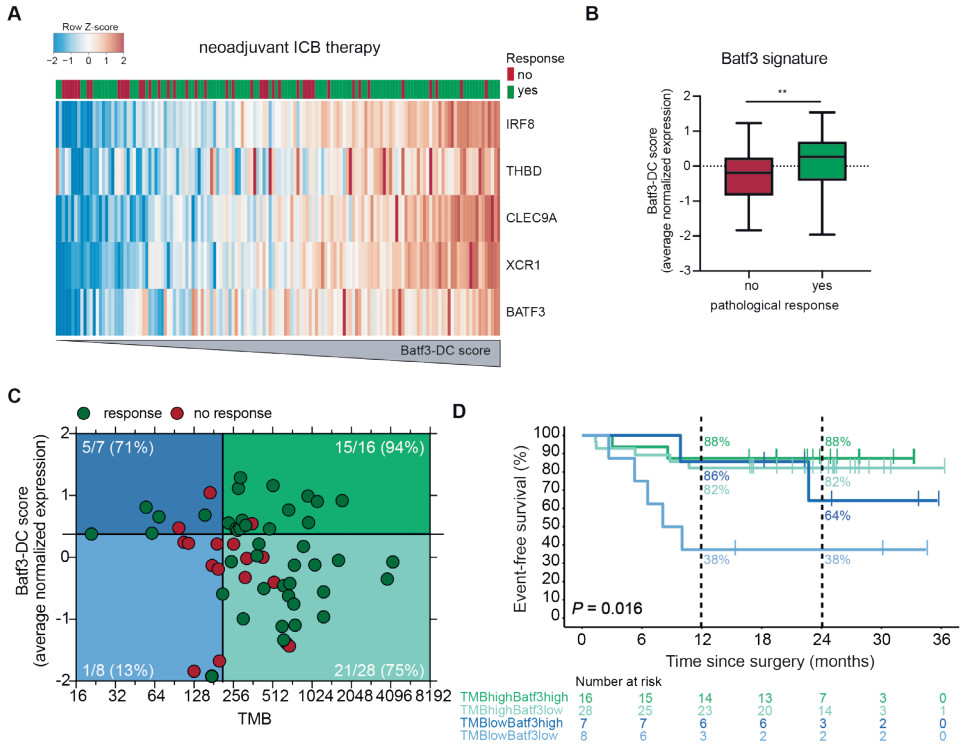

Figure 1 | Baseline Batf3-DC score is associated with pathological response of stage III melanoma patients treated with neoadjuvant ICB. (A-B) RNA sequencing of pre-treatment lymph node tumor biopsies of the OpACIN-neo and PRADO studies, including 144 patients for whom baseline material was available. **(A)** Heatmap of the Batf3 DC-associated RNA gene expression at baseline of patients ranked according to Batf3 DC-associated RNA gene signature expression score, which was calculated on the gene expression counts normalized by DESeq2. Each column represents one patient (green: response; red: no response) and rows display genes. **(B)** Batf3-DC score (average Z-score of Batf3 DC-associated gene signature expression) for patients with (green bar, n=101) or without (red bar, n=43) response (showing box and whiskers plot with min to max). *P* value was calculated using an unpaired Student's t test. **(C-D)** Patients of OpACIN-neo study for whom baseline tumor RNA sequencing and whole-exome sequencing data was available (n=59). Patients were grouped according to Batf3-DC score (average z-score of Batf3 DC-associated gene signature expression) and tumor mutational burden (TMB). Groups are determined by the optimal cutoff defined by the summary receiver characteristic (sROC) curves (cutoff for Batf3-DC score 0.3756; cutoff for TMB 212), resulting in a group with a low Batf3 gene signature expression score and low TMB (light blue), high Batf3 gene signature expression score and low TMB (dark blue), low Batf3 gene signature score and high TMB (light green) and high Batf3 gene signature expression score and high TMB (dark green). **(C)** TMB and Batf3-DC score for patients with a response (green dots) or without a response (red dots). **(D)** A Kaplan–Meier curve showing event-free survival (EFS) for different patient groups. *P* value was calculated using the log-rank test (two-sided) and is indicated. ** P < 0.01

To further assess the quality of the screen, Rainbow Calibration Particles were included on each plate to track data quality acquisition of the different lasers of the flow cytometer. We observed consistent signals of the different lasers during the acquisition of the data (**Figure S3D**). Next, we compared the normalized data distribution of the

three replicates of each screen plate. We found good correlations between most plate replicates; diverging plate replicates were excluded (4/63 plates) (**Figure S3E**).

To determine compounds that significantly enhance T cell proliferation after cross-presentation by DCs, we compared the number of proliferated $CD8^+$ T cells of the negative control (DMSO treated) to that exposed to the different compounds. Using a strictly standardized mean difference (SSMD) (47) of 3 or higher, we identified 145 compounds that significantly improved $CD8^+$ T cell proliferation after cross-presentation of tumor antigens by GM-CSF DCs (**Figure 2D**, **Figure S3F**, **Table S2**).

To further evaluate the effect of these 145 compounds on T cell activation and effector T cell induction, we determined the concentration of the proinflammatory cytokine IFN-γ in the supernatant at the end of the assay (**Figure 2E**, **Table S2**). Accordingly, we selected compounds that induced a significant increase in T cell proliferation combined with effective T cell activation, as measured by the IFN-γ concentration. The 145 selected compounds, that induced a significant increase in T cell proliferation, were ranked based on IFN-γ concentration in the supernatant. We selected the top 25 compounds with the highest measured IFN-γ for validation. We excluded the less suitable candidates Rose Bengal lactone (dye), corticosteroids (anti-inflammatory) and phosphoinositide 3-kinase (PI3K) inhibitors (recent clinical failure) (53). This strategy allowed us to identify 20 compounds that induced potent T cell activation after cross-presentation of tumor antigens by DCs.

AZD5582 increases T cell proliferation and proinflammatory cytokines

The screen identified 20 compounds of different chemical classes to significantly enhance $CD8^+$ T cell proliferation and IFN-γ secretion in the cross-presentation assay. We set out to validate these compounds by repeating the cross-presentation assay as in the screen, with the exception that we used a dose range (0.05 μM – 5 μM) or an expanded dose range (0.05 μM – 50 μM) for compounds for which saturation was not yet observed. This analysis confirmed that 11 compounds significantly improved $CD8^+$ T cell proliferation after cross-presentation of tumor antigens by GM-CSF DCs (**Figure 3A**, **Figure S4A, B**). A particularly strong effect was observed for the antagonist of inhibitor of apoptosis proteins (IAPs) AZD5582 (54), which resulted in a four-fold increase in $CD8^+$ T cell proliferation compared to DMSO control (**Figure 3A, B**). Furthermore, the concentration of released TNF was significantly increased by AZD5582 (**Figure 3C**), which was not observed for the other compounds (**Figure 3C**, **Figure S4C**). Moreover, the concentration of IL-2 significantly increased by AZD5582, indicative of effective T cell activation (**Figure 3D**). No change in the concentration of released DC-specific IL-12 was measured upon AZD5582 exposure (**Figure 3E**). The combination of high T cell

proliferation and secretion of effector cytokines demonstrated effective T cell activation by AZD5582. Therefore, we focused on AZD5582 for the remainder of this study.

The cross-presentation assay comprises different cell components (B16F10-OVA$^{B2m-/-}$ tumor cells, naïve CD8$^+$ T cells, GM-CSF DCs), which in principle could all be targeted by AZD5582. The goal of this study was to improve T cell proliferation by the induction of DC cross-presentation and therefore, we focused on DC-dependent effects. First, we pre-treated GM-CSF DCs with AZD5582 in the absence of both CpG ODN class B and B16F10-OVA$^{B2m-/-}$ tumor cells. After 24 hours of culture, the inhibitor was washed out and GM-CSF DCs were counted and used in the cross-presentation assay. Pre-treatment of GM-CSF DCs with AZD5582 resulted in a significant increase in CD8$^+$ T cell proliferation compared to control-treated GM-CSF DCs (**Figure 3F**). Next, to determine whether GM-CSF DCs were essential to induce T cell proliferation by AZD5582, they were excluded from the assay. In the absence of GM-CSF DCs, no significant increase in CD8$^+$ T cell proliferation was observed and no change in T cell viability was observed at most effective dose of AZD5582 (0.5 μM) (**Figure S5A-D**).

Antigen import and genes involved in cross-presentation are enhanced in DCs after AZD5582 treatment

To begin dissecting the mechanism by which AZD5582 stimulates DCs, we focused on endosome-to-cytosol import of antigens in DCs during cross-presentation. This transfer of exogenous antigens to the cytosol serves as one of the key steps of the cytosolic pathway of cross-presentation. Increased import has been proposed to improve cross-presentation of antigens sampled by DCs (55). To assess whether AZD5582 impacts on the efficiency of antigen import into the cytosol, we utilized the β-lactamase assay that allows to monitor the efficiency of antigen import into the cytosol. We first treated GM-CSF DCs for 24 hours with AZD5582 (0.5 μM), since we observed this increased T cell proliferation in a cross-presentation assay (**Figure 3F**). Efficient import of β-lactamase into the cytosol caused a disruption of fluorescence resonance energy transfer (FRET) by cleaving the β-lactam ring of CCF4 and consequently inducing a shift in fluorescence (**Figure 3G**). We observed enhanced antigen import when GM-CSF DCs were treated with AZD5582 (**Figure 3H, I**). In addition, H-2k^b (MHC class I) was expressed to higher levels on the surface of DCs after AZD5582 treatment (**Figure 3J**). We also observed that the transcripts of genes involved in the cross-presentation pathway (14) were significantly increased after AZD5582 treatment of DCs (**Figure 3K**). These findings, together with the observation that pre-treatment of GM-CSF DCs with AZD5582 induced enhanced T cell proliferation in a cross-presentation assay, suggest that the observed effect in the cross-presentation assay caused by AZD5582 involves a DC-dependent component.

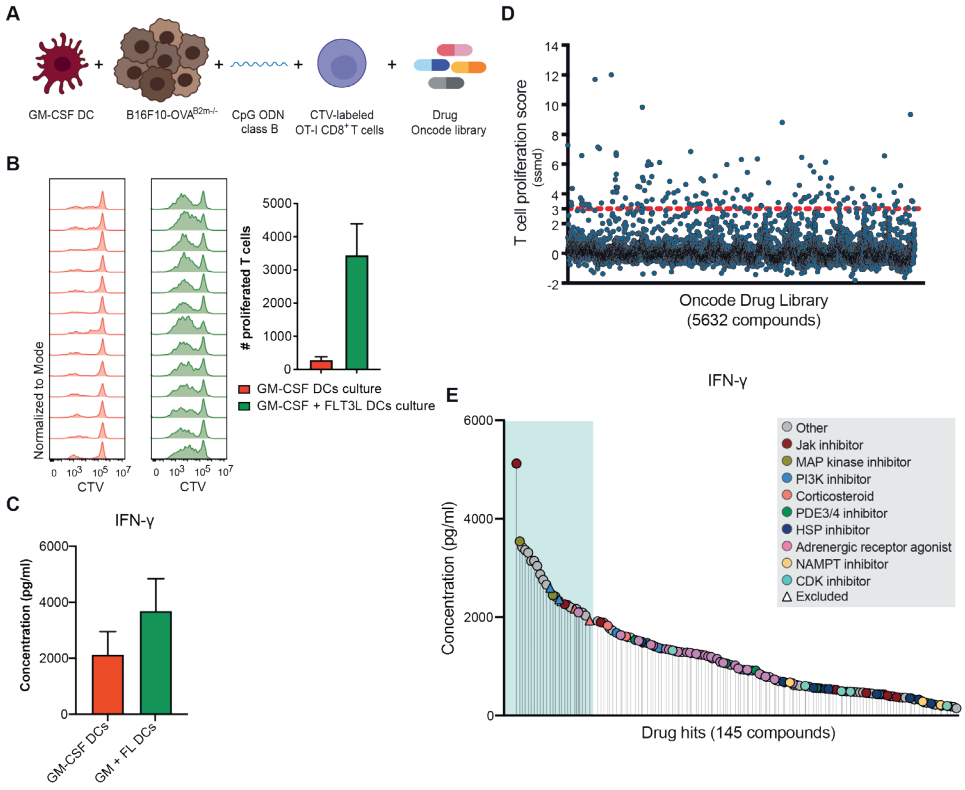

Figure 2 | Compound screen identifies 145 compounds to enhance T-cell proliferation after tumor antigen cross-presentation by DCs. (A) Overview of cross-presentation assay used for the compound screen: GM-CSF DCs, derived from bone marrow cells, were loaded with irradiated (100Gy) B16F10-OVA$^{B2m-/-}$ cells with the addition of CpG ODN class B (1 μM), CTV-labelled OT-I TCR specific CD8$^+$ T cells (10,000 cells each, 1:1:1) in the presence of Oncode Repurposing Drug Library (5632 compounds, dose: 0.5 μM). Number of proliferated CD8$^+$ T cells was assessed after 4 days by flow cytometery (iQue Screener). **(B)** Proliferated CD8$^+$ T cells for negative control (red; GM-CSF DCs loaded with irradiated (100Gy) B16F10-OVA$^{B2m-/-}$ cells, CpG ODN class B, OT-I TCR specific CD8$^+$ T cells in presence of 0.5 μM DMSO) and positive control (green; GM-CSF + FLT3L DCs loaded with irradiated (100Gy) B16F10-OVA$^{B2m-/-}$ cells, CpG ODN class B, OT-I TCR specific CD8$^+$ T cells in presence of 0.5 μM DMSO) for the compound screen. Representative flow cytometry histograms of CellTrace^{TM}Violet (CTV) dilution (left) and number of proliferated CD8$^+$ T cells (right) are shown (showing mean with SD). **(C)** Concentration of secreted IFN-γ as measured by CBA of the supernatant of the negative (red) and positive control (green) of the compound screen cross-presentation cultures (showing mean with SD). **(D)** The strictly standardized mean difference (SSMD)(47) for the different compounds (of the Oncode Repurposing Drug Library) was calculated based on the CD8$^+$ T-cell proliferation in cross-presentation assay. Each dot represents the SSMD of one compound (n=5632). For hit detection, a SSMD ≥ 3 was used, which is indicated by the red dotted line (n=145). **(E)** Concentration of IFN-γ secretion in the supernatant detected at the end of the cross-presentation assay (4 days) for the 145 hit compounds. The colors indicate different drug classes. The blue box indicates compounds that have been selected for further validation and the triangle compounds that have been excluded.

AZD5582 target engagement and activation of the non-canonical NF-kB pathway

To further dissect the mechanistic impact of AZD5582 on DCs, we analyzed (downstream) target signaling in DCs after AZD5582 treatment. AZD5582 is a second mitochondria-derived activator of caspases (SMAC) mimetic, binding to cIAP1 (*BIRC2*), cIAP2 (*BIRC3*) and XIAP (*BIRC4*), causing autoubiquitination and protein degradation (54). To determine whether AZD5582 has an on-target effect in DCs, we analyzed cell lysates of GM-CSF DCs that had been treated with various concentrations (0.1 μM – 1 μM) of AZD5582 by immunoblotting. After 24 hours of treatment with AZD5582, GM-CSF DCs showed a reduction in cIAP1, cIAP2 and XIAP expression (**Figure 4A**). A reduction in cIAP1 and cIAP2 was already observed after 2 hours, whereas the effect on XIAP was observed after 6 hours in a time course treatment with 0.5 μM AZD5582 (**Figure S6A**).

The cIAP proteins have been described to be key regulators of the non-canonical nuclear factor kappa B (NF-kB) pathway (56). To evaluate whether reduced expression of the cIAP proteins results in increased activation of the non-canonical NF-kB pathway, we analyzed the expression of NIK, p100 and p52. cIAP proteins control stability of NIK via ubiquitination and proteasomal degradation. Hence, lower levels of cIAP proteins should result in accumulation of NIK. After 24 hours of AZD5582 treatment, we indeed detected an accumulation of NIK in GM-CSF DCs (**Figure 4B**). In addition, downstream processing of the precursor p100 into the active p52 subunit was increased (**Figure 4B**). The observed enhanced activation of the non-canonical NF-kB pathway in DCs was detected already after 2 hours of treatment with AZD5582 (**Figure S6B**). Collectively, these data show that AZD5582 treatment has an on-target effect and triggers the downstream activation of the non-canonical NF-kB pathway in GM-CSF DCs.

Figure 3 | AZD5582 increases T-cell proliferation and proinflammatory cytokines after cross-presentation of tumor antigens by DCs. (A) Cross-presentation assay in the presence of AZD5582 (0.05 μM – 5 μM; blue dots) or DMSO controls (negative control: GM-CSF DCs, red dot; positive control: GM-CSF + FLT3L DCs, green dot) (n=5 biological replicates, each with 3 technical replicates. Plotted as mean with SEM). After 4 days, the number of CTV-diluted $CD8^+$ T cells was determined by flow cytometry. The number of proliferated $CD8^+$ T cells was normalized to the proliferating $CD8^+$ T cells of DMSO control (using GM-CSF DCs) within an experiment. *P* value was calculated using a one-way ANOVA with a Dunnett multiple comparisons test, comparing the negative control (GM-CSF DCs, without drug but DMSO) with the experimental well (dose of AZD5582). **(B)** Representative flow cytometry histograms for CTV dilution of viable $CD8^+$ T cells for DMSO control in GM-CSF + FLT3L culture (green) GM-CSF culture (red) and 0.5 μM AZD5582 in GM-CSF culture (blue) treatment. **(C-E)** Concentration of **(C)** TNF, **(D)** IL-2 and **(E)** IL-12p70 secretion was measured by CBA of supernatant of the cross-presentation assays as performed in (A) (n=4 biological replicates, each with 3-4 technical replicates. Plotted as mean with SEM). *P* value was calculated using a one-way ANOVA with a Dunnett multiple comparisons test, comparing the negative control (DMSO treated GM-CSF) and experimental well (dose of AZD5582). **(F)** GM-CSF DCs were pre-treated with either DMSO (red dot) or different concentrations of AZD5582 (0.1 μM – 1 μM; blue dots). After 24 hours, DCs were harvested, washed, counted and used in the cross-presentation as described in (A) without any addition. The number of proliferated $CD8^+$ T cells was normalized to the proliferated $CD8^+$ T cells of DMSO control within an experiment (n=3 biological replicates, each with 14 technical replicates. Plotted as mean with SEM). *P* value was calculated using a one-way ANOVA with a Dunnett multiple comparisons test, comparing the negative control (GM-CSF DCs, without drug but DMSO) and experimental well (dose of AZD5582). **(G-I)** β-lactamase assay to monitor efficiency of antigen import into the cytosol. **(G)** GM-CSF DCs were incubated with DMSO or 0.5 μM AZD5582 for 24 hours. After washing, DCs were incubated with β-lactamase for 3 hours, followed by CCF4 loading at room temperature for 30 minutes. **(H)** The percentage of cleaved off CCF4 in the cells was measured using flow cytometry, comparing DCs treated with DMSO (red bar) or 0.5 μM AZD5582 (blue bar) for 24 hours (n=5 biological replicates, each with 3 technical replicates, showing mean with SEM). *P* value was calculated using a paired Student's t test. **(I)** Representative flow cytometry data for the controls (no β-lactamase, no CCF4) and DMSO or AZD5582 treated GM-CSF DCs. **(J)** Expression of $H\text{-}2K^b$ (n=3 biological replicates, each with 3 technical replicates, showing mean with SEM) on pre-grated viable GM-CSF DCs was assessed by flow cytometry after treatment with DMSO (red bar) or different concentrations of AZD5582 (blue bars). Fold change of MFI was determined and within an experiment normalized to DMSO control expression. *P* value was calculated using a one-way ANOVA with a Dunnett multiple comparisons test, comparing between DMSO and AZD5582 treatment (for different doses). **(K)** RNA sequencing of GM-CSF DCs treated with AZD5582 (0.1 μM – 1 μM) or DMSO control for 24 hours. Normalized average gene expression of indicated genes of three biological replicates were plotted in the heatmap, comparing gene expression of DMSO control to indicated dose using a one-way ANOVA with a Dunnett multiple comparisons test. *, $P<0.05$, **, $P<0.01$, ***, $P<0.001$

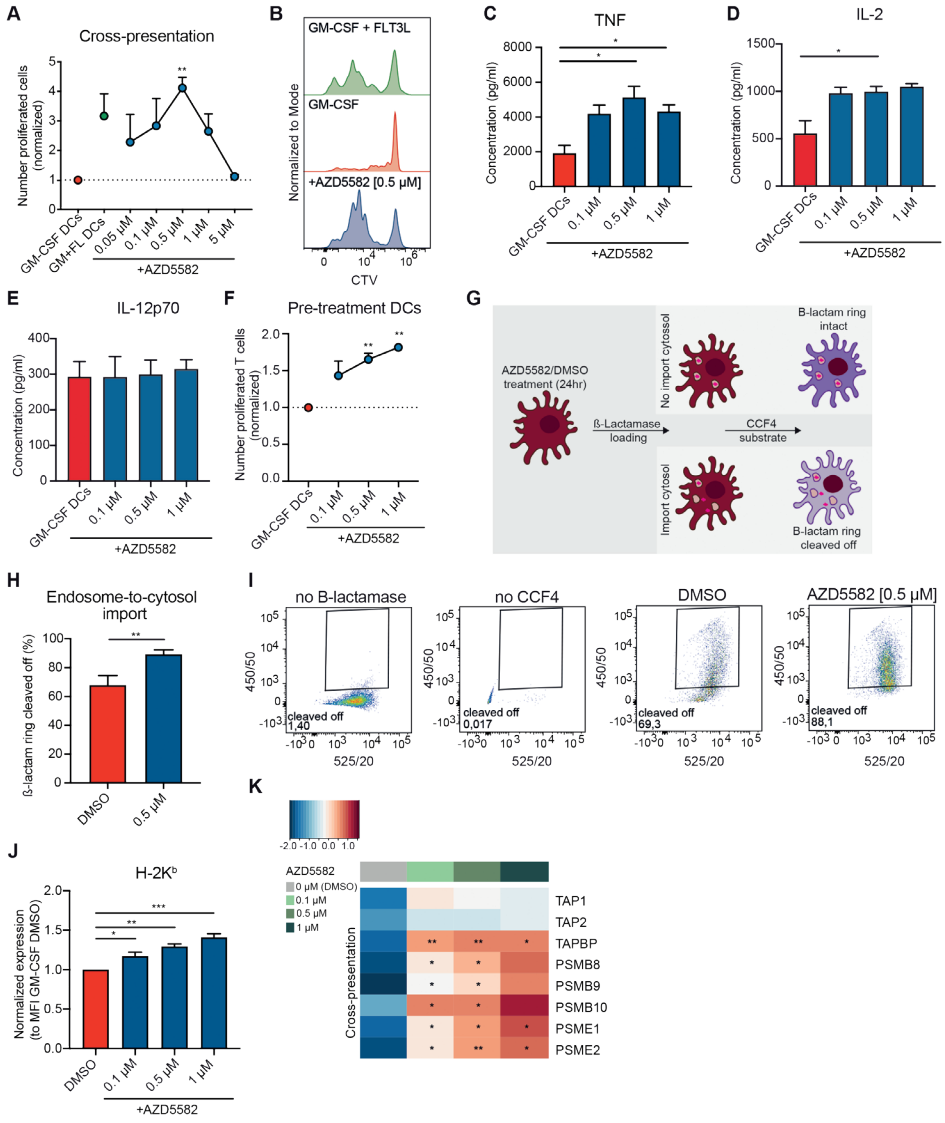

DC maturation and activation is stimulated by AZD5582

We next asked whether this increased activation of the non-canonical NF-kB pathway is accompanied by the maturation and activation of GM-CSF DCs (57). We analyzed GM-CSF DCs for several maturation and activation markers by flow cytometry after 24 hours of treatment with various concentrations of AZD5582. The population with high MHC class II and high CD86 expression significantly increased (**Figure 4C, D**), and a significant increase in the expression of CD80 and CD70 was also seen (**Figure 4E, F**). Moreover, at least 2-fold increases in these markers were observed, indicative of a strong effect on DC maturation by AZD5582. Furthermore, an increase in the expression of the

immune checkpoint markers programmed death-ligand 1 (PD-L1), PD-L2 and CD155 was observed (**Figure 4G-I**). AZD5582 also impacts C-C chemokine receptor type 7 (CCR7), a receptor important for trafficking to the lymph node and consequently cross-presentation of antigens to T cells (**Figure 4J**). In addition, we measured a significant increase in the concentration of released TNF (**Figure 4K**). An increased gene expression of other co-stimulatory molecules (CD40 and CD83) and proinflammatory cytokines (IL-6, IL-23A, IL-12B, IL-12A) was detected after AZD5582 treatment of DCs (**Figure 4L**). These data indicate that AZD5582 treatment stimulates GM-CSF DC maturation and activation.

To expand upon this, we assessed if these markers were also upregulated in other DC subsets by AZD5582. Treatment of GM-CSF + FLT3L DCs with AZD5582 in a cross-presentation assay resulted only in a trend of increased T cell proliferation at low dose (0.05 μM) (**Figure S7A**). These GM-CSF + FLT3L DCs showed higher baseline expression of the activation markers compared to GM-CSF DCs and AZD5582 induced significant increase in the expression of CD80 and CD86 (**Figure S7B-E**). The expression of the cDC1 specific marker, chemokine receptor XCR1, was significantly increased by AZD5582 treatment (**Figure S7F**), which was not observed for GM-CSF DCs. An increased expression of genes involved in cross-presentation, co-stimulation and cytokines was also observed when GM-CSF + FLT3L DCs were treated with AZD5582 (**Figure S7G**). In addition, we analyzed whether *in vivo* differentiated Pan-DCs (including both cDCs and plasmacytoid DCs) were altered by AZD5582 treatment. Pan-DCs were also able to upregulate the expression of MHC class II, CD86, CD80 and CD70 after 24 hours *ex vivo* treatment with AZD5582, although the effect size was smaller compared to bone marrow derived GM-CSF DCs (**Figure S7H-K**). In addition, we observed that AZD5582 also significantly increases the efficiency of antigen import into the cytosol of Pan-DCs, $XCR1^+$ DCs and $PDCA1^+$ DCs, whereas there was no effect on cross-presentation by $SIRPa^+$ (**Figure S7L-O**). To explore the potential human relevance of these findings, we treated moDCs obtained from healthy donor PBMCs with AZD5582 for 24 hours. Despite a high expression of the maturation and activation markers at baseline in moDCs, an increase in $CD80^{high}CD86^{high}$ population and CD70 expression was observed (**Figure 4M,N**). In addition, an increased gene expression of the co-stimulatory receptors as well as co-inhibitory receptors was detected after treatment of human moDCs (**Figure 4O**). Together, these data show that AZD5582 treatment induces maturation and activation of both mouse and human DCs.

In vivo vaccination model for testing AZD5582

Next, we studied the effect of AZD5582 treatment on DC function and $CD8^+$ T cell proliferation in an *in vivo* vaccination model. C57BL/6JRj mice were injected (i.v.) with naïve CTV-labeled $CD8^+$ T cells obtained from OT-I donor mice. The following day, irradiated $B16F10^{B2m-/-}$ cells with or without OVA expression and CpG class B were co-injected (i.v.), together with AZD5582 or vehicle control (i.p.) (**Figure S8A, B**). In this setting, which closely resembles our *in vitro* cross-presentation assay, only tumor antigens that have been processed to SIINFEKL and presented in the context of H-$2k^b$ by antigen presenting cells (e.g. DCs) can induce activation and proliferation of OT-I TCR-specific $CD8^+$ T cells. After five days, we found that compared to vehicle-treated mice, mice receiving AZD5582 had a substantial increase of $CD80^+$ DCs (**Figure S8C-E**). The increase in $CD80^+$ DCs upon AZD5582 treatment was not specific to the tumor antigen, since we also observed this in mice that received $B16F10^{B2m-/-}$ cells without the expression of OVA (**Figure S8H, I**). While AZD5582 induced a significant increase in the number of proliferated $CD8^+$ T cells *in vitro* (**Figure 3A**), this increase was less pronounced in this *in vivo* model. No change in the percentage of antigen-specific ($SIINFEKL^+$) $CD8^+$ T cells upon AZD5582 treatment was observed (**Figure S8F**). We found that AZD5582-treated mice had a minor but significant increase in proliferated $CD8^+$ T cells as measured by CTV dilution (**Figure S8G**). There was almost an absence of antigen-specific $CD8^+$ T cells and CTV dilution for mice receiving $B16F10^{B2m-/-}$ cells without the expression of OVA, and this was not affected by the treatment of AZD5582 (**Figure S8J, K**).

To determine the effect of AZD5582 in a tumor vaccination model, we challenged mice with s.c. injection of different number of tumor cells (10,000, 100,000 or 1,000,000) on day 3 of this vaccination model (**Figure S8A**). We observed that injection of 10,000 cells failed to establish a tumor (**Figure S8L**). When higher numbers of tumor cells were injected, we did observe tumor outgrowth. No difference in outgrowth of 1,000,000 tumor cells was observed between vehicle and AZD5582-treated mice. However, mice injected with 100,000 cells showed increased tumor outgrowth when pre-treated with AZD5582 compared to vehicle control. All outgrowing tumors ($CD45^-$ population), ranging in size between 144 – 3034 mm^3, lacked cell surface expression of H-$2K^b$, while the $CD45^+$ population showed H-$2K^b$ expression (**Figure S8M**). This data indicates that all the outgrowing tumors lacked MHC class I expression and can therefore not be recognized by the activated $CD8^+$ T cells. In addition, all these mice had tumor cells in their spleens, indicating metastasis formation. We conclude that, due to lack of MHC I expression and therefore these tumors could not be controlled by $CD8^+$ T cells, this is not an optimal model to study improved tumor control through increased immune activation.

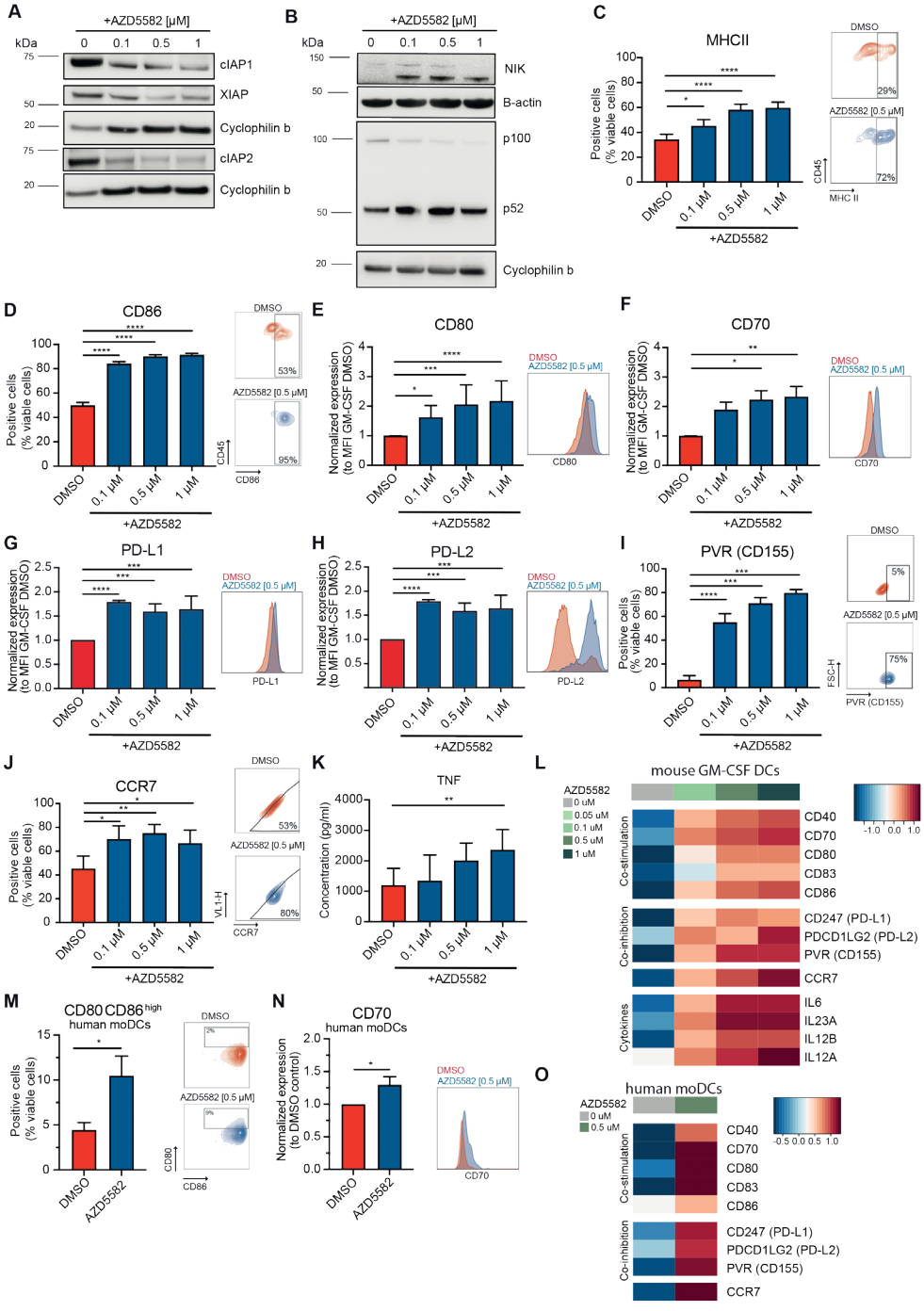
A
+AZD5582 [μM]
kDa
0 0.1 0.5 1
75
cIAP1
XIAP
50
20
Cyclophilin b
75
cIAP2
20
Cyclophilin b
B
+AZD5582 [μM]
kDa
0 0.1 0.5 1
150
NIK
50
B-actin
100
p100
50
p52
20
Cyclophilin b
C
MHCII
Positive cells (% viable cells)
DMSO
0.1 μM
0.5 μM
1 μM
+AZD5582
DMSO
29%
AZD5582 [0.5 μM]
72%
CD45
MHC II
D
CD86
Positive cells (% viable cells)
DMSO
AZD5582 [0.5 μM]
53%
95%
CD45
CD86
E
CD80
Normalized expression (to MFI GM-CSF DMSO)
DMSO
AZD5582 [0.5 μM]
CD80
F
CD70
Normalized expression (to MFI GM-CSF DMSO)
DMSO
AZD5582 [0.5 μM]
CD70
G
PD-L1
Normalized expression (to MFI GM-CSF DMSO)
DMSO
AZD5582 [0.5 μM]
PD-L1
H
PD-L2
Normalized expression (to MFI GM-CSF DMSO)
DMSO
AZD5582 [0.5 μM]
PD-L2
I
PVR (CD155)
Positive cells (% viable cells)
DMSO
5%
AZD5582 [0.5 μM]
75%
FSC-H
PVR (CD155)
J
CCR7
Positive cells (% viable cells)
DMSO
53%
AZD5582 [0.5 μM]
80%
VL1-H
CCR7
K
TNF
Concentration (pg/ml)
L
mouse GM-CSF DCs
AZD5582
0 uM
0.05 uM
0.1 uM
0.5 uM
1 uM
-1.0 0.0 1.0
Co-stimulation
CD40
CD70
CD80
CD83
CD86
Co-inhibition
CD247 (PD-L1)
PDCD1LG2 (PD-L2)
PVR (CD155)
CCR7
Cytokines
IL6
IL23A
IL12B
IL12A
M
CD80 CD86 high
human moDCs
Positive cells (% viable cells)
DMSO
AZD5582
DMSO
2%
AZD5582 [0.5 μM]
9%
CD80
CD86
N
CD70
human moDCs
Normalized expression (to DMSO control)
DMSO
AZD5582
DMSO
AZD5582 [0.5 μM]
CD70
O
human moDCs
AZD5582
0 uM
0.5 uM
-0.5 0.0 0.5 1.0
Co-stimulation
CD40
CD70
CD80
CD83
CD86
Co-inhibition
CD247 (PD-L1)
PDCD1LG2 (PD-L2)
PVR (CD155)
CCR7

Figure 4 | Upregulation of non-canonical NF-kB pathway and induction of DC maturation after treatment with AZD5582. (A) The expression of cIAP1, cIAP2, XIAP and downstream signaling proteins of the non-canonical NF-kB pathway **(B)** NIK and p52/p100 by GM-CSF DCs after AZD5582 treatment (0.1 μM – 1 μM; or DMSO negative control) for 24 hours was assessed by western blotting. Cyclophilin b or β-actin was used as loading control. **(C-J)** Surface marker analysis of GM-CSF DCs after AZD5582 treatment (0.1 μM – 1 μM; or DMSO negative control) for 24 hours. The expression of **(C)** MHC class II (n=10 biological replicates, each with 2-3 technical replicates, showing mean with SEM), **(D)** CD86 (n=10 biological replicates, each with 2-3 technical replicates, showing mean with SEM), **(E)** CD80 (n=10 biological replicates, each with 2-3 technical replicates, showing mean with SEM), **(F)** CD70 (n=7 biological replicates, each with 3 technical replicates, showing mean with SEM), **(G)** PD-L1 (n=4 biological replicates, each with 3 technical replicates, showing mean with SEM), **(H)** PD-L2 (n=4 biological replicates, each with 3 technical replicates, showing mean with SEM), **(I)** PVR (CD155) (n=4 biological replicates, each with 3 technical replicates, showing mean with SEM), **(J)** CCR7 (n=4 biological replicates, each with 3 technical replicates, showing mean with SEM) on pre-gated viable GM-CSF DCs was assessed by flow cytometry after treatment with DMSO (red bar) or different concentrations of AZD5582 (blue bars), including representative flow cytometry plots and gating strategy for DMSO control (red) and AZD5582 (0.5 μM); blue). (C-D, I-J) Percentage positive cells was determined and (E-H) MFI was determined and within an experiment normalized to DMSO control expression. *P* value was calculated using a one-way ANOVA with a Dunnett multiple comparisons test, comparing between DMSO and AZD5582 treatment (for different doses). **(K)** Concentration of TNF secretion was measured by CBA of the supernatant of DCs treated with DMSO (red bar) or AZD5582 (0.1 μM – 1 μM; blue bars). *P* value was calculated using paired Student's t test between DMSO and AZD5582 treatment (for different doses) (n=3-4 biological replicates, each with 3-4 technical replicates, showing mean with SEM). Statistical analysis was performed by one-way ANOVA with a Dunnett multiple comparisons test. **(L)** RNA sequencing of GM-CSF DCs treated with AZD5582 (0.1 μM – 1 μM) or DMSO control for 24 hours. Normalized average gene expression of indicated genes of three biological replicates were plotted in the heatmap. **(M-N)** Expression of (M) $CD80^{high}CD86^{high}$ and (N) CD70 on human moDCs after treatment with DMSO (red bar) or AZD552 (0.5 μM; blue bar) was assessed by flow cytometry. Right: representative flow cytometry plots and gating strategy for DMSO control (red) and AZD5582 (blue). (M) A paired Student's t test and (N) unpaired Student's t test between DMSO and AZD5582 was used to determine significance (n=4 biological replicates, each with 2-3 technical replicates, showing mean with SEM). *P* value is indicated above the bars. **(O)** RNA sequencing of human moDCs treated with AZD5582 (0.5 μM) or DMSO control for 24 hours. Normalized average gene expression of indicated genes of three healthy human donors were plotted in the heatmap. *, $P<0.05$, **, $P<0.01$, ***, $P<0.001$, ****, $P<0.0001$

AZD5582 + anti-PD-1 combination therapy reduces MC38 tumor outgrowth and improves survival

We next asked whether AZD5582 treatment has a beneficial effect in a tumor setting. As we observed an increase in expression of the co-inhibitory molecules, including PD-L1/2, upon AZD5582 treatment, we assessed whether ICB therapy could increase a T cell-mediated anti-tumor immune response and further improve outcome. C57BL/6JRj mice were s.c. injected with syngeneic B16F10-OVA tumor cells. When the average tumor size reached 100 mm^3, mice received anti-PD-1 and/or anti-CTLA-4 (or the corresponding isotype control) in combination with AZD5582 (or vehicle control) (**Figure S9A**). A week after treatment, satellite mice were harvested to analyze the immune populations in the tumors and spleens.

Treating mice with ICB with or without AZD5582 did not induce a significant increase in tumor antigen-specific ($SIINFEKL^+$) $CD8^+$ T cells in the tumor (**Figure S9B**), while a significant increase in $SIINFEKL^+$ $CD8^+$ T cells was observed in the draining lymph node and spleen (**Figure S9C, D**), showing a significant increase for combination therapy of

AZD5582 + anti-PD-1 compared to monotherapy. While $CD8^+$ T cells in the spleen and draining lymph node showed higher expression of the activation marker CD69 upon treatment with AZD5582, no increase in the activation of $CD8^+$ T cells (based on CD69 and CD137 expression) in tumor was observed for any treatment (**Figure S9E-H**). In the draining lymph node, no significant increase in the cross-presenting $XCR1^+$ DC population (58) was observed when mice were treated with AZD5582 or anti-PD-1 alone, however, this was the case in the treatment combination groups (**Figure S9I**). In addition, treating mice with AZD5582 (with or without ICB) induced a significant increase in $CD86^+$ and $CD80^+$ mostly on $CD11b^+$MHC II^+ DCs (**Figure S9J-M**).

The tumor outgrowth was significantly reduced in all treatment groups compared to vehicle + isotype control (**Figure S9N**). Treatment with AZD5582 alone reduced tumor outgrowth significantly and showed a beneficial survival compared to control. However, despite the systemic increase of tumor-specific $CD8^+$ T cells by combining AZD5582 with ICB, this did not translate into an additive reduction in tumor outgrowth or improved survival (**Figure S9N-P**)

Lastly, we used the MC38 colorectal tumor model (**Figure 5A**), which showed to be anti-PD-1 non-responsive using the indicated treatment scheme (**Figure 5A-C**). In this model, AZD5582 treatment augmented the response to anti-PD-1, showing a significant reduction in tumor outgrowth as well as a significant improvement in survival for AZD5582 + anti-PD-1 treatment compared to control or anti-PD-1 monotherapy (**Figure 5B-D**). Altogether, these results confirm previous evidence that AZD5582 has antitumor activity and stimulates DCs (59), but also indicates that AZD5582 could potentially improves the efficacy of immunotherapy in an anti-PD-1 non-responsive model.

Discussion

Cross-presentation of tumor antigens by DCs is crucial for the initiation of tumor-specific $CD8^+$ T cell responses, and thereby critical for effective anti-tumor immune responses (13-20). In this study, we developed a strategy to find compounds that could enhance the capacity of BMDCs (GM-CSF DCs) to prime and induce $CD8^+$ T cell proliferation after cross-presentation of tumor antigens. We performed a high-throughput pharmacological screen using over 5,500 compounds to identify enhancers of $CD8^+$ T cell proliferation after cross-presentation of tumor antigens by DCs. We found 145 compounds that significantly enhance T cell proliferation after cross-presentation by DCs. We further focused on compounds that in addition also increased IFN-γ secretion, because of its (direct and indirect) anti-tumor properties (60, 61). Of the selected compounds, a total of 11 compounds were confirmed to significantly enhance $CD8^+$ T cell proliferation.

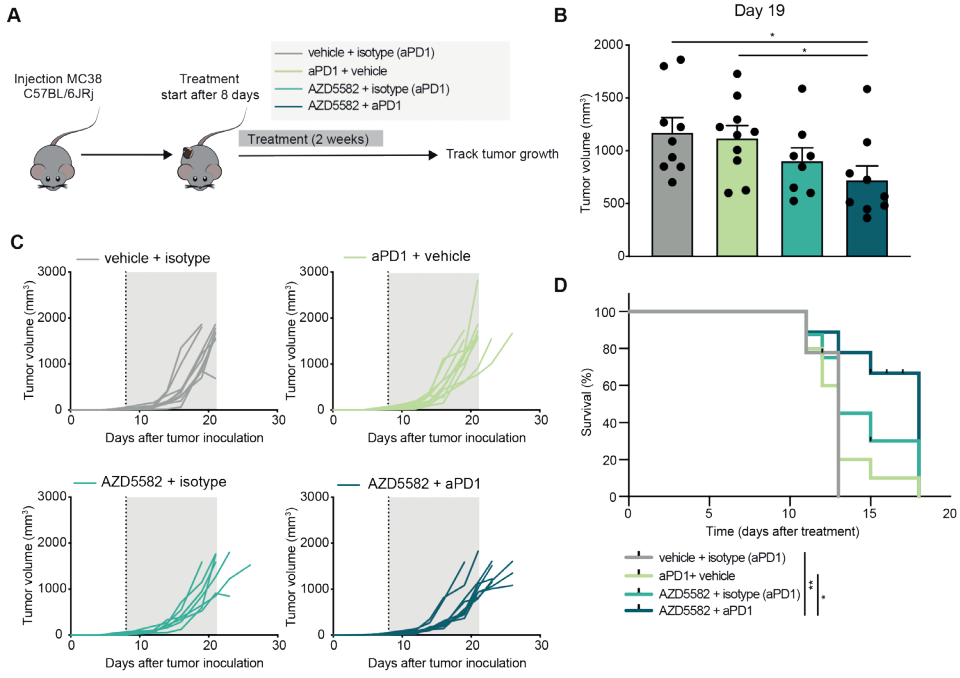

Figure 5 | AZD5582 reduces MC38 tumor outgrowth and improves survival in combination with anti–PD-1 therapy. (A) C57BL/6JRj mice were injected with MC38 cells (0.5 x 10^6 on the right flank). On day 8, mice were treated with vehicle + isotype control, anti–PD-1 (100 µg, i.p. two times per week), AZD5582 (0.5 mg/kg, i.v. three times per week) + isotype control or combination of anti–PD-1 + AZD5582 for 2 weeks. **(B)** Tumor volume on day 19 (8 days after treatment), showing mean with SEM. An unpaired Student's t test comparing the different treatment groups was used to determine significance. **(C)** Individual tumor growth curves for different treatment groups, the start of treatment is indicated with a dotted line and lasts 2 weeks (indicated by grey area). **(D)** Kaplan–Meier survival curve of all mice. Statistical testing was performed by Long-rank test. *P* value is indicated above the bars. *, $P<0.05$, **, $P<0.01$

The strongest effect on T cell proliferation after cross-presentation of tumor antigens by DCs was found upon AZD5582 exposure, an antagonist of the IAPs. Moreover, an increased secretion of IFN-γ, TNF and IL-2 was detected, indicating effective T cell activation. While AZD5582 might have exerted additional effect on other cell components of the cross-presentation assay (tumor cells and T cells), we observed an important role for DCs. For cross-presentation by DCs, exogenous tumor antigens are engulfed and processed (12). For the cytosolic pathway, antigens are imported into the cytosol, followed by proteasomal degradation and peptide loading on MHC class I in the endoplasmic reticulum (62-64). The cytosolic export of internalized antigens is a rate-limiting step for efficient cross-presentation of tumor antigens (19, 55). Here, we observed that AZD5582 indeed promotes antigen export to the cytosol and increases the expression of genes involved in cross-presentation. In addition, AZD5582 activated the non-canonical NF-kB pathway in DCs, resulting in increased NIK expression, which

in turn has been demonstrated to be critical for efficient antigen cross-presentation (65, 66). Together, these findings implicate that AZD5582 enhances the capacity of GM-CSF DCs to cross-present antigens, potentially owing to NF-kB pathway activation.

Efficient T cell priming, expansion and reactivation rely on co-stimulatory signals provided by antigen-presenting cells (APCs). Co-stimulation via CD28 on T cells by interaction with CD80 and CD86 on APCs, has been shown to be a crucial step for T cell activation (67, 68). The importance of the provision of co-stimulatory molecules is further emphasized by studies showing that infiltration of DCs, especially matured DCs, is important for response to ICB (15, 16). Here, we consistently observe that AZD5582 induces increased expression of co-stimulatory molecules CD80 and CD86 on DCs (across all DC subtypes tested *in vitro* and *in vivo*). Furthermore, AZD5582 treatment also increased expression of CD70, MHC class II, CCR7, PD-L1, PD-L2, CD155 and the secretion of TNF, indicating proper DC maturation and activation. In line with this, AZD5582 was previously found to enhance IL-12 production by DCs using a reporter mouse system (59). We found an increase in IL-12 gene expression in DCs, but were unable to detect increased IL-12 in the supernatant. This might be due immediate T cell usage of the secreted IL-12, which in turn could be detected using a reporter mouse system (59). These observations together imply that AZD5582 induces maturation and activation of DCs.

We planned to test AZD5582 in a tumor vaccination model, in which mice were vaccinated (i.v.) with B16F10-OVA$^{B2m-/-}$ cells, to study tumor antigen cross-presentation. However, this model appeared to be confounded: we found tumor cells in the spleen of these mice, likely from the vaccination step. Although the i.v. injected tumor cells had been irradiated and were confirmed to be incapable of proliferation *in vitro*, it is possible that a few surviving cells might have migrated to the spleen. That these cells lacked B2m expression may have contributed to this, since they cannot be recognized and killed by CD8$^+$ T cells. In addition, we observed that the transplanted tumors of AZD5582 pre-treated mice grew out faster, despite a higher degree of systemic immune activation. All outgrowing tumors had lost MHC class I expression, and therefore also these cells could not be recognized by the CD8$^+$ T cells. It has been described that a high immune pressure results in cancer immunoediting, thereby resulting in loss of antigen presentation, and a consequent escape from CD8$^+$ T cell mediated killing (69). It is conceivable that the fast outgrowth of tumor cells in AZD5582-treated mice could be attributed to increased effector immune pressure, thereby leading to stronger selection against antigen expressing tumor cells. These confounding factors made it difficult to draw definitive conclusions about the translational potential of AZD5582 in the adjuvant setting at this point.

AZD5582, like other IAP inhibitors, has been developed to induce apoptosis in cancer cells and has an antitumor effect in different tumor models (54, 59). Here, we observed that AZD5582 also increased DC and $CD8^+$ T-cell activation *in vitro*. We therefore tested AZD5582 in combination with anti–PD-1 in B16F10-OVA melanoma and MC38 colorectal tumor models. While the combination of AZD5582 with anti–PD-1 increased the frequency of systemic antigen-specific $CD8^+$ T cells compared to anti–PD-1 monotherapy, no additional effect of combining AZD5582 with anti–PD-1 was observed in B16F10-OVA tumor outgrowth and survival. In contrast, in MC38 tumor bearing mice, which in our hands had no response to single anti–PD-1 treatment, the addition of AZD5582 significantly reduced tumor outgrowth and improved survival. Although we observed increased T-cell and DC activation systemically, we have not formally excluded that a direct tumor killing has contributed, at least in part, to our *in vivo* observations. An experiment in mice that lack DCs or have DCs hampered in cross-presentation, using CD11c-DTR (70), XCR1-DTR (71) or $Batf3^{-/-}$ (13) mice, could give more insight into the DC-dependency of AZD5582 in tumor control.

Our results indicate that addition of AZD5582 might be beneficial in PD-1-refractory late-stage disease, but might be inefficient or even counterproductive in a PD-1-sensitive or early-stage disease, respectively. In line with this notion, previous work has shown that cross-presentation of tumor antigens by DCs plays an important role in the reinvigoration of dysfunctional $CD8^+$ T cells after ICB therapy (14, 16, 21). Infiltration of the specialized cross-presenting cDC1 has been shown to correlate with increased clinical response to ICB therapy (21). To add to this, we showed that the presence of cDC1s (as measured by the Batf3-score) within the tumor is also associated with response when ICB therapy is given prior to surgery, which we previously also found in a smaller patient cohort (22). Therefore, patients that currently do not respond to ICB therapy could potentially benefit from strategies to enhance T cell priming and expansion.

In conclusion, here we reported several small molecules that could boost antigen cross-presentation, in particular AZD5582. Although AZD5582 is in a pre-clinical development stage, other IAP inhibitors are being tested in combination with ICB therapy in clinical trials (NCT03270176, NCT04122625, NCT03871959, NCT03111992, NCT02587962, NCT03166631). It would be of interest to evaluate whether these therapeutic regimens also enhance DC maturation and expand tumor-specific T cells. Taken together, an approach targeting cross-presentation could be of benefit for patients that do not respond to ICB therapy. Our high-throughput screening strategy identifies compounds that enhance T cell proliferation after cross-presentation which could provide opportunities to find new therapeutics.

Acknowledgement

This work was financed in large part by an MRA Team Science Award (681127) awarded to D.S. Thommen, D.S. Peeper, and C.U. Blank.Wethank all members of the Blank, Peeper, Schumacher, Thommen, Kvistborg, and Voest group for scientific support and valuable discussions. We thank the Preclinical Intervention Unit, Olaf van Tellingen and Artur Burylo, for their input and technical support for animal experiments.Wethank Ton Schumacher for breeding and sharing the OT-Imice, and Mireille Toebes and Ton Schumacher for providing the fluorescence conjugated H- 2Kb-SIINFEKL tetramer. We thank Serge Zander for the animal pathology support and input. We thank Juan Zhou and Duy Minh Le for their technical support. We thank Martijn van Baalen and Frank van Diepen for input for flow cytometry use for screening. We thank the NKI–AVL facilities for their technical support: Core Facility Molecular Pathology and Biobanking, Flow Cytometry facility, Animal Laboratory and Animal Pathology facility. We thank the Oncode Institute for providing us with the Drug Repurposing Library.

Author contributions

E.P.H. and C.U.B conceived the project. E.P.H., D.R., B.M., R.L.B., M.A.L. and R.L. performed the screen. P.D., H.S. and C.L. performed bioinformatic analyses. J.A.S. and P.T.R. performed *in vivo* experiments. E.P.H. and P.T.R. performed all other experiments. E.A.R. and I.L.M.R. provided clinical data. E.P.H, D.S.P. and C.U.B. wrote the manuscript. All authors revised and approved the manuscript. The project was supervised by D.S.P. and C.U.B.

Financial support

This work was financed in large part by an MRA Team Science Award (681127) awarded to D. S. Thommen, D. S. Peeper and C. U. Blank.

Declaration of interests

M.A. Ligtenberg reports other support from Immagene outside the submitted work. C.U. Blank reports advisory role: BMS, MSD, Roche, Novartis, GSK, AZ, Pfizer, Lilly, GenMab, Pierre Fabre, Third Rock Ventures; and reports research funding from BMS, Novartis, NanoString, 4SC; and Stockownership: cofounder Immagene BV and Signature Oncology; as well as reports patents (including submitted): WO 2021/177822 A1, N2027907, and P091040NL2. No disclosures were reported by the other authors.

References

1. Topalian SL, Hodi FS, Brahmer JR, Gettinger SN, Smith DC, McDermott DF, et al. Safety, Activity, and Immune Correlates of Anti–PD-1 Antibody in Cancer. New England Journal of Medicine. 2012;366(26):2443-54.
2. Hodi FS, O'Day SJ, McDermott DF, Weber RW, Sosman JA, Haanen JB, et al. Improved survival with ipilimumab in patients with metastatic melanoma. New England Journal of Medicine. 2010;363(8):711-23.
3. Schadendorf D, Hodi FS, Robert C, Weber JS, Margolin K, Hamid O, et al. Pooled analysis of long-term survival data from phase II and phase III trials of ipilimumab in unresectable or metastatic melanoma. Journal of clinical oncology. 2015;33(17):1889.
4. Larkin J, Chiarion-Sileni V, Gonzalez R, Grob JJ, Cowey CL, Lao CD, et al. Combined nivolumab and ipilimumab or monotherapy in untreated melanoma. New England journal of medicine. 2015;373(1):23-34.
5. Larkin J, Chiarion-Sileni V, Gonzalez R, Grob J-J, Rutkowski P, Lao CD, et al. Five-year survival with combined nivolumab and ipilimumab in advanced melanoma. New England Journal of Medicine. 2019;381(16):1535-46.
6. Wolchok JD, Chiarion-Sileni V, Gonzalez R, Rutkowski P, Grob J-J, Cowey CL, et al. Overall survival with combined nivolumab and ipilimumab in advanced melanoma. New England Journal of Medicine. 2017;377(14):1345-56.
7. Hodi FS, -Sileni VC, Lewis KD, Grob J-J, Rutkowski P, Lao CD, et al. Long-term survival in advanced melanoma for patients treated with nivolumab plus ipilimumab in CheckMate 067. Journal of Clinical Oncology. 2022;40(16_suppl):9522-.
8. Blank CU, Rozeman EA, Fanchi LF, Sikorska K, van de Wiel B, Kvistborg P, et al. Neoadjuvant versus adjuvant ipilimumab plus nivolumab in macroscopic stage III melanoma. Nature medicine. 2018;24(11):1655-61.
9. Rozeman EA, Menzies AM, van Akkooi AC, Adhikari C, Bierman C, van de Wiel BA, et al. Identification of the optimal combination dosing schedule of neoadjuvant ipilimumab plus nivolumab in macroscopic stage III melanoma (OpACIN-neo): a multicentre, phase 2, randomised, controlled trial. The Lancet Oncology. 2019;20(7):948-60.
10. Menzies AM, Amaria RN, Rozeman EA, Huang AC, Tetzlaff MT, van de Wiel BA, et al. Pathological response and survival with neoadjuvant therapy in melanoma: a pooled analysis from the International Neoadjuvant Melanoma Consortium (INMC). Nature Medicine. 2021;27(2):301-9.
11. Tumeh PC, Harview CL, Yearley JH, Shintaku IP, Taylor EJM, Robert L, et al. PD-1 blockade induces responses by inhibiting adaptive immune resistance. Nature. 2014;515(7528):568-71.
12. Heath WR, Belz GT, Behrens GM, Smith CM, Forehan SP, Parish IA, et al. Cross-presentation, dendritic cell subsets, and the generation of immunity to cellular antigens. Immunological reviews. 2004;199(1):9-26.
13. Hildner K, Edelson BT, Purtha WE, Diamond M, Matsushita H, Kohyama M, et al. Batf3 deficiency reveals a critical role for CD8α+ dendritic cells in cytotoxic T cell immunity. Science. 2008;322(5904):1097-100.
14. Broz Miranda L, Binnewies M, Boldajipour B, Nelson Amanda E, Pollack Joshua L, Erle David J, et al. Dissecting the Tumor Myeloid Compartment Reveals Rare Activating Antigen-Presenting Cells Critical for T Cell Immunity. Cancer Cell. 2014;26(5):638-52.
15. Spranger S, Bao R, Gajewski TF. Melanoma-intrinsic β-catenin signalling prevents anti-tumour immunity. Nature. 2015;523(7559):231-5.
16. Salmon H, Idoyaga J, Rahman A, Leboeuf M, Remark R, Jordan S, et al. Expansion and activation of CD103+ dendritic cell progenitors at the tumor site enhances tumor responses to therapeutic PD-L1 and BRAF inhibition. Immunity. 2016;44(4):924-38.
17. Sánchez-Paulete AR, Cueto FJ, Martínez-López M, Labiano S, Morales-Kastresana A, Rodríguez-Ruiz ME, et al. Cancer immunotherapy with immunomodulatory anti-CD137 and anti–PD-1 monoclonal antibodies requires BATF3-dependent dendritic cells. Cancer discovery. 2016;6(1):71-9.
18. Spranger S, Dai D, Horton B, Gajewski TF. Tumor-Residing Batf3 Dendritic Cells Are Required for Effector T Cell Trafficking and Adoptive T Cell Therapy. Cancer Cell. 2017;31(5):711-23.e4.
19. Theisen DJ, Davidson IV JT, Briseño CG, Gargaro M, Lauron EJ, Wang Q, et al. WDFY4 is required for cross-presentation in response to viral and tumor antigens. Science. 2018;362(6415):694-9.

20. Alloatti A, Rookhuizen DC, Joannas L, Carpier J-M, Iborra S, Magalhaes JG, et al. Critical role for Sec22b-dependent antigen cross-presentation in antitumor immunity. Journal of Experimental Medicine. 2017;214(8):2231-41.
21. Barry KC, Hsu J, Broz ML, Cueto FJ, Binnewies M, Combes AJ, et al. A natural killer–dendritic cell axis defines checkpoint therapy–responsive tumor microenvironments. Nature Medicine. 2018;24(8):1178-91.
22. Liu J, Rozeman EA, O'Donnell JS, Allen S, Fanchi L, Smyth MJ, et al. Batf3+ DCs and type I IFN are critical for the efficacy of neoadjuvant cancer immunotherapy. Oncoimmunology. 2019;8(2):e1546068.
23. Brunner C, Seiderer J, Schlamp A, Bidlingmaier M, Eigler A, Haimerl W, et al. Enhanced Dendritic Cell Maturation by TNF-α or Cytidine-Phosphate-Guanosine DNA Drives T Cell Activation In Vitro and Therapeutic Anti-Tumor Immune Responses In Vivo. The Journal of Immunology. 2000;165(11):6278-86.
24. Sánchez-Paulete AR, Teijeira Á, Quetglas JI, Rodríguez-Ruiz ME, Sánchez-Arráez Á, Labiano S, et al. Intratumoral Immunotherapy with XCL1 and sFlt3L Encoded in Recombinant Semliki Forest Virus-Derived Vectors Fosters Dendritic Cell-Mediated T-cell Cross-Priming. Cancer Res. 2018;78(23):6643-54.
25. Ribas A, Medina T, Kirkwood JM, Zakharia Y, Gonzalez R, Davar D, et al. Overcoming PD-1 blockade resistance with CpG-A toll-like receptor 9 agonist vidutolimod in patients with metastatic melanoma. Cancer Discovery. 2021;11(12):2998-3007.
26. Hammerich L, Marron TU, Upadhyay R, Svensson-Arvelund J, Dhainaut M, Hussein S, et al. Systemic clinical tumor regressions and potentiation of PD1 blockade with in situ vaccination. Nature medicine. 2019;25(5):814-24.
27. Bonifaz L, Bonnyay D, Mahnke K, Rivera M, Nussenzweig MC, Steinman RM. Efficient targeting of protein antigen to the dendritic cell receptor DEC-205 in the steady state leads to antigen presentation on major histocompatibility complex class I products and peripheral CD8+ T cell tolerance. J Exp Med. 2002;196(12):1627-38.
28. Caminschi I, Proietto AI, Ahmet F, Kitsoulis S, Shin Teh J, Lo JCY, et al. The dendritic cell subtype-restricted C-type lectin Clec9A is a target for vaccine enhancement. Blood. 2008;112(8):3264-73.
29. Sancho D, Mourão-Sá D, Joffre OP, Schulz O, Rogers NC, Pennington DJ, et al. Tumor therapy in mice via antigen targeting to a novel, DC-restricted C-type lectin. J Clin Invest. 2008;118(6):2098-110.
30. Ott PA, Hu Z, Keskin DB, Shukla SA, Sun J, Bozym DJ, et al. An immunogenic personal neoantigen vaccine for patients with melanoma. Nature. 2017;547(7662):217-21.
31. Rozeman E, Hoefsmit E, Reijers I, Saw R, Versluis J, Krijgsman O, et al. Survival and biomarker analyses from the OpACIN-neo and OpACIN neoadjuvant immunotherapy trials in stage III melanoma. Nature Medicine. 2021:1-8.
32. Reijers ILM, Menzies AM, van Akkooi ACJ, Versluis JM, van den Heuvel NMJ, Saw RPM, et al. Personalized response-directed surgery and adjuvant therapy after neoadjuvant ipilimumab and nivolumab in high-risk stage III melanoma: the PRADO trial. Nature Medicine. 2022.
33. Dobin A, Davis CA, Schlesinger F, Drenkow J, Zaleski C, Jha S, et al. STAR: ultrafast universal RNA-seq aligner. Bioinformatics. 2013;29(1):15-21.
34. Anders S, Pyl PT, Huber W. HTSeq—a Python framework to work with high-throughput sequencing data. bioinformatics. 2015;31(2):166-9.
35. Durinck S, Spellman PT, Birney E, Huber W. Mapping identifiers for the integration of genomic datasets with the R/Bioconductor package biomaRt. Nature protocols. 2009;4(8):1184-91.
36. Love MI, Huber W, Anders S. Moderated estimation of fold change and dispersion for RNA-seq data with DESeq2. Genome biology. 2014;15(12):1-21.
37. Becht E, Giraldo NA, Lacroix L, Buttard B, Elarouci N, Petitprez F, et al. Estimating the population abundance of tissue-infiltrating immune and stromal cell populations using gene expression. Genome biology. 2016;17(1):1-20.
38. Danaher P, Warren S, Dennis L, D'Amico L, White A, Disis ML, et al. Gene expression markers of tumor infiltrating leukocytes. Journal for immunotherapy of cancer. 2017;5(1):1-15.
39. Li H, Durbin R. Fast and accurate short read alignment with Burrows–Wheeler transform. bioinformatics. 2009;25(14):1754-60.
40. Van der Auwera GA, Carneiro MO, Hartl C, Poplin R, Del Angel G, Levy-Moonshine A, et al. From FastQ data to high-confidence variant calls: the genome analysis toolkit best practices pipeline. Current protocols in bioinformatics. 2013;43(1):11.0. 1-.0. 33.
41. Vredevoogd ea. No Title Manuscript under Preparation. n.d. .

42. Vredevoogd DW, Kuilman T, Ligtenberg MA, Boshuizen J, Stecker KE, de Bruijn B, et al. Augmenting immunotherapy impact by lowering tumor TNF cytotoxicity threshold. Cell. 2019;178(3):585-99. e15.
43. Zhang Z, Kong X, Ligtenberg MA, van Hal-van Veen SE, Visser NL, de Bruijn B, et al. RNF31 inhibition sensitizes tumors to bystander killing by innate and adaptive immune cells. Cell Reports Medicine.
44. Mayer CT, Ghorbani P, Nandan A, Dudek M, Arnold-Schrauf C, Hesse C, et al. Selective and efficient generation of functional Batf3-dependent CD103+ dendritic cells from mouse bone marrow. Blood, The Journal of the American Society of Hematology. 2014;124(20):3081-91.
45. Corsello SM, Bittker JA, Liu Z, Gould J, McCarren P, Hirschman JE, et al. The Drug Repurposing Hub: a next-generation drug library and information resource. Nature medicine. 2017;23(4):405-8.
46. Zhang J-H, Chung TD, Oldenburg KR. A simple statistical parameter for use in evaluation and validation of high throughput screening assays. Journal of biomolecular screening. 1999;4(2):67-73.
47. Zhang XD. A pair of new statistical parameters for quality control in RNA interference high-throughput screening assays. Genomics. 2007;89(4):552-61.
48. Ali M, Foldvari Z, Giannakopoulou E, Böschen M-L, Strønen E, Yang W, et al. Induction of neoantigen-reactive T cells from healthy donors. Nature protocols. 2019;14(6):1926-43.
49. Edgar R, Domrachev M, Lash AE. Gene Expression Omnibus: NCBI gene expression and hybridization array data repository. Nucleic acids research. 2002;30(1):207-10.
50. Blank CU, Reijers ILM, Pennington T, Versluis JM, Saw RP, Rozeman EA, et al. First safety and efficacy results of PRADO: A phase II study of personalized response-driven surgery and adjuvant therapy after neoadjuvant ipilimumab (IPI) and nivolumab (NIVO) in resectable stage III melanoma. Journal of Clinical Oncology. 2020;38(15_suppl):10002-.
51. Joffre OP, Segura E, Savina A, Amigorena S. Cross-presentation by dendritic cells. Nature Reviews Immunology. 2012;12(8):557-69.
52. Hogquist KA, Jameson SC, Heath WR, Howard JL, Bevan MJ, Carbone FR. T cell receptor antagonist peptides induce positive selection. Cell. 1994;76(1):17-27.
53. Algazi AP, Rotow J, Posch C, Ortiz-Urda S, Pelayo A, Munster PN, et al. A dual pathway inhibition strategy using BKM120 combined with vemurafenib is poorly tolerated in BRAF V600(E/K) mutant advanced melanoma. Pigment Cell Melanoma Res. 2019;32(4):603-6.
54. Hennessy EJ, Adam A, Aquila BM, Castriotta LM, Cook D, Hattersley M, et al. Discovery of a novel class of dimeric Smac mimetics as potent IAP antagonists resulting in a clinical candidate for the treatment of cancer (AZD5582). Journal of medicinal chemistry. 2013;56(24):9897-919.
55. Kozik P, Gros M, Itzhak DN, Joannas L, Heurtebise-Chrétien S, Krawczyk PA, et al. Small molecule enhancers of endosome-to-cytosol import augment anti-tumor immunity. Cell reports. 2020;32(2):107905.
56. Varfolomeev E, Blankenship JW, Wayson SM, Fedorova AV, Kayagaki N, Garg P, et al. IAP antagonists induce autoubiquitination of c-IAPs, NF-κB activation, and TNFα-dependent apoptosis. Cell. 2007;131(4):669-81.
57. Sun S-C. Non-canonical NF-κB signaling pathway. Cell Research. 2011;21(1):71-85.
58. Bachem A, Hartung E, Güttler S, Mora A, Zhou X, Hegemann A, et al. Expression of XCR1 characterizes the Batf3-dependent lineage of dendritic cells capable of antigen cross-presentation. Front Immunol. 2012;3:214.
59. Garris CS, Arlauckas SP, Kohler RH, Trefny MP, Garren S, Piot C, et al. Successful anti-PD-1 cancer immunotherapy requires T cell-dendritic cell crosstalk involving the cytokines IFN-γ and IL-12. Immunity. 2018;49(6):1148-61. e7.
60. Barth RJ, Jr, Mulé JJ, Spiess PJ, Rosenberg SA. Interferon gamma and tumor necrosis factor have a role in tumor regressions mediated by murine CD8+ tumor-infiltrating lymphocytes. Journal of Experimental Medicine. 1991;173(3):647-58.
61. Gao J, Shi LZ, Zhao H, Chen J, Xiong L, He Q, et al. Loss of IFN-γ Pathway Genes in Tumor Cells as a Mechanism of Resistance to Anti-CTLA-4 Therapy. Cell. 2016;167(2):397-404.e9.
62. Kovacsovics-Bankowski M, Rock K. A phagosome-to-cytosol pathway for exogenous antigens presented on MHC class I molecules. Science. 1995;267(5195):243-6.
63. Ackerman AL, Kyritsis C, Tampé R, Cresswell P. Early phagosomes in dendritic cells form a cellular compartment sufficient for cross presentation of exogenous antigens. Proceedings of the National Academy of Sciences. 2003;100(22):12889-94.
64. Guermonprez P, Saveanu L, Kleijmeer M, Davoust J, Van Endert P, Amigorena S. ER–phagosome fusion defines an MHC class I cross-presentation compartment in dendritic cells. Nature. 2003;425(6956):397-402.

65. Katakam AK, Brightbill H, Franci C, Kung C, Nunez V, Jones C, et al. Dendritic cells require NIK for CD40-dependent cross-priming of CD8+ T cells. Proceedings of the National Academy of Sciences. 2015;112(47):14664-9.
66. Yu H, Lin L, Zhang Z, Zhang H, Hu H. Targeting NF-κB pathway for the therapy of diseases: mechanism and clinical study. Signal transduction and targeted therapy. 2020;5(1):1-23.
67. Hui E, Cheung J, Zhu J, Su X, Taylor MJ, Wallweber HA, et al. T cell costimulatory receptor CD28 is a primary target for PD-1–mediated inhibition. Science. 2017;355(6332):1428-33.
68. Kamphorst AO, Wieland A, Nasti T, Yang S, Zhang R, Barber DL, et al. Rescue of exhausted CD8 T cells by PD-1–targeted therapies is CD28-dependent. Science. 2017;355(6332):1423-7.
69. Schreiber RD, Old LJ, Smyth MJ. Cancer Immunoediting: Integrating Immunity’s Roles in Cancer Suppression and Promotion. Science. 2011;331(6024):1565-70.
70. Jung S, Unutmaz D, Wong P, Sano G, De los Santos K, Sparwasser T, et al. In vivo depletion of CD11c+ dendritic cells abrogates priming of CD8+ T cells by exogenous cell-associated antigens. Immunity. 2002;17(2):211-20.
71. Yamazaki C, Sugiyama M, Ohta T, Hemmi H, Hamada E, Sasaki I, et al. Critical Roles of a Dendritic Cell Subset Expressing a Chemokine Receptor, XCR1. The Journal of Immunology. 2013;190(12):6071-82.

Supplemental information

Table 1 | List of the reagents used

Reagent or Resource	Source	Cat no.
Antibodies FACS (mouse)		
CD3e-FITC (clone 145-2C11) (1:200)	Thermo Fisher	11-0031-85
CD3e-PE-Dazzle594 (clone 145-2C11) (1:200)	BioLegend	100347
CD3e-PE-Cyanine7 (clone 17A2) (1:400)	BioLegend	100220
CD3e-PE (clone 145-2C11) (1:400)	BioLegend	100308
CD11b-APC-Cyanine7 (clone M1/70) (1:400)	BioLegend	101226
CD11b-FITC (clone M1/70) (1:100)	BD Biosciences	553310
CD11c-APC-Cyanine7 (clone N418) (1:200)	BioLegend	117323
CD11c-BV785 (clone N418) (1:200)	BioLegend	117335
CD11c-Pacific Blue (clone N418) (1:200)	BioLegend	117321
CD11c-PE/Vio770 (clone N418) (1:100)	Miltenyi Biotec	130-120-223
CD155 (PVR)-PE (clone 4.24.1) (1:100)	BioLegend	132205
CD16/32 Fc Block (clone 93) (1:400)	Thermo Fisher	14-0161-85
CD172a (SIRP-alpha)-PerCP-eFluor710 (clone p84) (1:100)	Thermo Fisher	46-1721-82
CD197 (CCR7, EBI-1)-PE (clone 2E9/CCL5) (1:100)	Thermo Fisher	12-1971-82
CD273 (B7-DC, PD-L2)-BV421 (clone TY25) (1:100)	BioLegend	107219
CD274 (B7-H1, PD-L1)-PE (clone MIH5) (1:100)	Thermo Fisher	12-5982-83
CD4-BV785 (clone GK1.5) (1:200)	BioLegend	100453
CD45.2-FITC (clone 104) (1:200)	BioLegend	109806
CD45.2-APC (clone 104) (1:200)	Thermo Fisher	17-0454-82
CD69-PE/Dazzle592 (clone H1.2F3) (1:100)	BioLegend	104535
CD8a-PerCP-efluor710 (Clone 53-6.7) (1:400)	Thermo Fisher	46-0081-82
CD8a-PE (Clone53-6.7) (1:400)	Thermo Fiser	12-0081-83
CD70-PE-Cyanine7 (clone FR70) (1:100)	BioLegend	104612
CD70-PE (clone FR70) (1:100)	BioLegened	104605
CD80(B7-1)-eFluor450 (Clone 16-10A1) (1:200)	Thermo Fisher	48-0801-80
CD80(B7-1)-FITC (clone 16-10A1) (1:400)	Thermo Fisher	11-0801-82
CD86-PE (clone GL-1) (1:500)	BioLegend	105008
CD137-APC (clone 17B5-1H1) (1:400)	Miltenyi Biotec	130-102-515
CD279 (PD-1)-eFluor450 (clone J43) (1:100)	Thermo Fisher	48-9985-82
CD317 (PDCA-1)-APC (clone JF05-1C2.4.1) (1:100)	Miltenyi Biotec	130-123-789
MHCI (H-2K^{b})-PE-Cyanine7 (clone AF6.88.5.5.3) (1:100)	Thermo Fisher	25-5958-82
MHCI (H-2K^{b})-Pacific Blue (clone AF6.88.5) (1:200)	BioLegend	116514
MHCII (I-A/I-E)-PerCP-efluor710 (clone M5/114.15.2) (1:800)	Thermo Fisher	46-5321-82
MHCII (I-A/I-E)-PE (clone M5/114.15.2) (1:1200)	BD Biosciences	557000
NK1.1-PE-Dazzle594 (clone PK136) (1:200)	BioLegend	108747

$OVA_{257-264}$ (SIINFEKL) peptide bound to H-2K^b (clone: 25-D1.16)	In-house developed	
XCR1-APC (clone REA707) (1:100)	Miltenyi Biotec	130-111-373
XCR1-PE (clone REA707) (1:100)	Miltenyi Biotec	130-111-184
Antibodies FACS (human)		
CD11c-FITC (clone 3.9) (1:200)	BioLegend	301603
CD14-Pacific Blue (clone HCD14) (1:200)	BioLegend	325615
CD70-PE (clone 113-16) (1:200)	BioLegend	355103
CD80-PE (clone 2D10) (1:200)	BioLegend	305207
CD86-Pacific Blue (clone IT2.2) (1:200)	BioLegend	305417
HLA-DR-Pacific Blue (clone LN3) (1:200)	BioLegend	327016
Antibodies Western Blot		
Anti-cIAP1(Rabbit/IgG)	Abcam	ab154525
Anti-cIAP2 (315304) (Mouse/IgG_1)	R&D systems	MAB817
Anti-XIAP (Rabbit/IgG)	Cell Signaling	2042
Anti-cyclophilin B (D1V5J) (Rabbit/IgG)	Cell Signaling	43603
Anti-β-Actin (D6A8) (Rabbit/IgG)	Cell Signaling	8457
Anti-p100/p52 (Rabbit/IgG)	Cell Signaling	4882
Anti-NIK (Rabbit/IgG)	Cell Signaling	CST4994T
Anti-Hsp90 (Clone 68/Hsp90) (Mouse IgG)	BD Biosciences	610419
HRP-conjugated anti-mouse IgG (Goat)	Thermo Fisher	G-21040
HRP-conjugated anti-Rabbit IgG (Goat)	Thermo Fisher	G-21234
Chemicals, peptides, Recombinant Proteins and other reagents		
Recombinant Murine Granulocyte Macrophage Colony Stimulating Factor (rm GM-CSF, 50ug)	Immunotools	12343125
Mouse Flt3 Ligand (Flt3L), recombinant Protein, Invitrogen (10ug)	Fisher Scientific	11554970
Human recombinant Granulocyte Macrophage Colony Stimulating Factor (GM-CSF)	Peprotech	300-03
Human recombinant IL-4	Peprotech	200-04
CpG oligonucleotides class B (ODN 1826 – TLR9 ligand)	Invivogen	Tlrl-1826-5
Hygromycin B	Invitrogen	10687010
Rainbow Calibration Particles, 8 peaks	BioLegend	422903
Pan Dendritic Cell Isolation Kit	Miltenyi Biotec	130-100-875
$CD8a^+$ T cell isolation kit	Miltenyi Biotec	130-104-075
CD14 MicroBeads	Miltenyi Biotec	130-050-201
AZD5582	MedChemExpress	HY-12600
AZD5582	Selleck Chem	S7362
Filgotinib	MedChemExpress	HY-18300
Brigatinib	MedChemExpress	HY-12857
Gilteritinib	MedChemExpress	HY-12432
ERK5-IN-1	MedChemExpress	HY-14403
Solcitinib	MedChemExpress	HY-16755

Arglabin	MedChemExpress	HY-16059
R112	MedChemExpress	HY-16420
Oxydefrine	Key Organics	KS-1460
TC-ASK-10	Tocris	4825
PD-407824	Tocris	2694
SB-612111	Tocris	3573
SCH-28080	Tocris	1690
2-Pyrimidinecarbonitrile	Sigma Aldrich	646830
Dioscin (Collettiside III)	SelleckChem	S2379
PF-0056227	SelleckChem	S2672
BX-912	SelleckChem	S1275
VU 0357121	SelleckChem	S2795
LGK-974	SelleckChem	S7143
ML347	SelleckChem	S7148
Critical Commercial Assays		
LIVE/DEAD™ Fixable Near-IR Dead Cell Stain Kit	Thermo Fisher	L34976
LIVE/DEAD™ Fixable Yellow Dead Cell Stain Kit	Thermo Fisher	L34968
BD™ Cytometric Bead Array (CBA) Mouse IL-12p70 Flex Set	BD Biosciences	558303
BD™ Cytometric Bead Array (CBA) Mouse IFNy Flex Set	BD Biosciences	558296
BD™ Cytometric Bead Array (CBA) Mouse TNF Flex Set	BD Biosciences	558299
BD™ Cytometric Bead Array (CBA) Mouse IL-2 Flex Set	BD Biosciences	558297
CellTrace™ Violet Cell Proliferation Kit	ThermoFisher	C34557

Table S2 | Compound hits identified by cross-presentation screen

Ranking	Name	*P* value	SSMD	FDR	IFN-γ (pg/ml)	Included validation
1	17-AAG (Tanespimycin)	0.00057	12	0.0606	685	
2	Ruxolitinib (INCB018424)	0.00541	11.7	0.194	557	
3	Baricitinib (LY3009104)	0.00084	9.83	0.0736	192	
4	Retaspimycin (Hydrochloride)	0.000941	9.34	0.0737	1504	
5	S-Ruxolitinib	0.000891	8.81	0.0736	495	
6	CYCLOSPORINE	0.00000000191	7.27	0.000000827	718	
7	broxaterol	0.0066	7.15	0.209	736	
8	Salmeterol (xinafoate)	0.000242	7.05	0.0337	1225	
9	CNX-774	0.00608	6.85	0.203	1921	
10	PIK-75	0.000326	6.76	0.0399	434	
11	Bardoxolone Methyl	0.000444	6.59	0.0521	272	
12	Dolastin-10	0.019	6.58	0.351	1030	
13	OTSSP167 (hydrochloride)	0.000155	6.55	0.0236	390	

14	Decernotinib	0.00219	6.46	0.114	1361	
15	17-DMAG HCl (Alvespimycin)	0.00000000364	6.36	0.00000146	353	
16	SNX-2112	0.0000711	6.31	0.0129	543	
17	PF-04929113 (SNX-5422)	0.00171	6.15	0.104	246	
18	BKM120 (NVP-BKM120)	0.00217	6.14	0.114	1377	
19	Onalespib (AT13387)	0.000505	6.11	0.0558	487	
20	NVP-HSP990	0.000891	5.96	0.0736	564	
21	Gandotinib (LY2784544)	0.0179	5.96	0.344	524	
22	NVP-BGT226	2.52E-41	5.91	2.37E-38	219	
23	BIIB021	0.00138	5.9	0.0893	435	
24	TC-ASK-10	0.00296	5.48	0.145	3539	X
25	N-Methyldopamine·HCl	0.00131	5.45	0.0878	1342	
26	MK-8776 (SCH 900776)	0.00584	5.33	0.201	1404	
27	YM-58483	0.000458	5.21	0.0526	1057	
28	oxyfedrine	0.000733	5.17	0.0695	2098	X
29	zilpaterol	0.0242	5.11	0.38	1203	
30	AZD5582	0.0397	5.07	0.48	3363	X
31	Tacrolimus	0.00212	5.06	0.114	350	
32	Solcitinib	0.00554	5.02	0.194	2261	X
33	ALBUTEROL	0.0277	4.97	0.404	658	
34	XL888	0.00266	4.9	0.131	324	
35	Lirimilast	0.000258	4.88	0.0346	914	
36	CZC-54252	0.0261	4.85	0.391	619	
37	Tofacitinib (CP-690550. Tasocitinib)	0.0064	4.76	0.208	434	
38	rolipram-R(-)	0.00401	4.76	0.169	1477	
39	Entospletinib (GS-9973)	0.0246	4.64	0.381	531	
40	Arglabin	0.00722	4.58	0.22	2165	X
41	TULOBUTEROL HYDROCHLORIDE	0.00000599	4.56	0.00169	1441	
42	Gilteritinib	0.00741	4.53	0.222	3423	X
43	Harringtonine	0.00148	4.52	0.0937	232	
44	Omaveloxolone (RTA-408)	0.0045	4.47	0.176	201	
45	KX2-391	0.0141	4.46	0.304	605	
46	CGP-60474	0.00119	4.43	0.0824	486	
47	ERK5-IN-1	0.00435	4.41	0.175	2447	X
48	Actinomycin D	0.000477	4.37	0.0537	433	
49	dinoprostone	0.00000678	4.36	0.00174	539	
50	PD-407824	0.00562	4.36	0.195	2660	X
51	Zilpaterol·HCl	0.00456	4.31	0.177	1286	

52	anisomycin	0.000159	4.27	0.0236	368	
53	MG-132	0.00173	4.23	0.104	366	
54	Filgotinib	0.0073	4.2	0.22	5122	X
55	Plicamycin (Mithramycin)	0.00113	4.12	0.0824	325	
56	NECA	0.000273	4.11	0.0349	916	
57	CLENBUTEROL HYDROCHLORIDE	0.00308	4.1	0.147	1278	
58	Omipalisib (GSK2126458. GSK458)	0.00534	4.08	0.194	263	
59	CYT997	0.0344	4.07	0.448	785	
60	formoterol	0.00782	4.06	0.229	1635	
61	Cebranopadol	0.00357	4.05	0.16	1595	
62	dipivefrine	0.00472	4.05	0.181	1353	
63	Ethylnorepinephrine (hydrochloride)	0.00436	4.04	0.175	1311	
64	procaterol	0.00103	4	0.0784	1192	
65	Bortezomib	0.00178	3.97	0.106	483	
66	SB-612111	0.00763	3.96	0.227	2091	X
67	Gambogic Acid	0.0035	3.94	0.159	482	
68	TERBUTALINE HEMISULFATE	0.000589	3.88	0.0614	1019	
69	NSC-663284	0.00662	3.86	0.209	1287	
70	CEFALONIUM	0.00301	3.85	0.146	1269	
71	STF-118804	0.0176	3.85	0.342	216	
72	rolipram-S(+)	0.00422	3.84	0.172	1535	
73	Diacetoxyscirpenol	0.00407	3.84	0.169	452	
74	BMS-649	0.00952	3.82	0.246	1771	
75	Dioscin (Collettiside III)	0.00141	3.81	0.0902	2869	X
76	RGB-286638 (free base)	0.0412	3.76	0.489	196	
77	Wortmannin	0.0252	3.75	0.383	2596	
78	Ixazomib Citrate (MLN9708)	0.00644	3.74	0.208	588	
79	Levalbuterol hydrochloride	0.0114	3.73	0.271	849	
80	trans-4-[8-(3-Fluorophenyl)-1.7-naphthyridin-6-yl] cyclohexanecarboxylic-acid	0.00549	3.73	0.194	1061	
81	FLUMETHAZONE PIVALATE	0.00553	3.72	0.194	1829	
82	HOKU-81	0.0068	3.7	0.212	1298	

83	ISOPROTERENOL HYDROCHLORIDE	0.00442	3.7	0.175	792	
84	Ixazomib citrate	0.00000892	3.67	0.00218	175	
85	Bruceantin	0.00631	3.67	0.208	393	
86	DACTINOMYCIN	0.00395	3.63	0.169	552	
87	DL-Adrenaline	0.0529	3.62	0.542	1295	
88	rose-bengal-lactone	0.00162	3.6	0.0992	2324	
89	Ansamitocin P-3	0.0315	3.58	0.426	147	
90	PF-00562271	0.0019	3.56	0.108	2247	X
91	VU 0357121 __ VU 0357121 __ VU 0357121	0.0135	3.55	0.296	2201	X
92	ADRENALONE HYDROCHLORIDE	0.000994	3.54	0.0767	1484	
93	Triptolide	0.0000636	3.54	0.0119	477	
94	FK-866	0.00769	3.54	0.227	286	
95	Ilginatinib hydrochloride	0.00623	3.51	0.206	375	
96	DESOXYMETASONE	0.00805	3.51	0.234	1240	
97	RITODRINE HYDROCHLORIDE	0.0353	3.5	0.454	932	
98	Ixazomib (MLN2238)	0.0372	3.48	0.471	676	
99	NYLIDRIN HYDROCHLORIDE	0.00725	3.48	0.22	1253	
100	TG101209	0.0377	3.48	0.472	1626	
101	BRL-37344	0.00247	3.47	0.126	957	
102	AZD8186	0.00913	3.46	0.246	1677	
103	DEXAMETHASONE SODIUM PHOSPHATE	0.000913	3.45	0.0736	1931	
104	XMD17-109	0.00881	3.44	0.242	832	
105	AZ 960	0.00933	3.42	0.246	459	
106	alvocidib	0.00475	3.4	0.181	496	
107	ISOETHARINE MESYLATE	0.0112	3.39	0.271	1151	
108	Brilliant Green	0.0047	3.36	0.181	597	
109	DEXAMETHASONE ACETATE	0.0000000000486	3.34	0.0000000249	2174	
110	Dinaciclib (SCH727965)	0.00232	3.33	0.12	602	
111	ML347	0.0109	3.33	0.268	3143	X
112	EMETINE DIHYDROCHLORIDE	0.0247	3.33	0.381	185	
113	LGK-974	0.0164	3.32	0.329	3041	X
114	Carfilzomib (PR-171)	0.00134	3.31	0.0884	471	
115	HYDROCORTISONE VALERATE	0.00000668	3.31	0.00174	1425	
116	PREDNISOLONE ACETATE	0.000115	3.3	0.018	1608	

117	Oprozomib (ONX 0912)	0.00648	3.29	0.209	448	
118	Vilanterol (trifenatate)	0.0069	3.28	0.212	1520	
119	AMCINONIDE	0.00123	3.28	0.0835	941	
120	CH5132799	0.033	3.27	0.439	914	
121	WYE-125132	0.000645	3.26	0.0649	471	
122	BMS-536924	0.0102	3.26	0.256	783	
123	Hexoprenaline sulphate	0.0275	3.25	0.403	1075	
124	Apremilast (CC-10004) __ Apremilast (CC-10004)	0.0132	3.24	0.293	934	
125	CC-292 (AVL-292)	0.0319	3.24	0.429	1889	
126	ETP-45658	0.0147	3.23	0.308	2362	
127	homoharringtonine	0.00603	3.23	0.203	618	
128	Peficitinib (ASP015K. JNJ-54781532)	0.0126	3.23	0.286	406	
129	BX-912	0.00158	3.22	0.0978	2033	X
130	GPP-78	0.0098	3.19	0.251	675	
131	Entrectinib (RXDX-101)	0.0532	3.18	0.542	1583	
132	kenpaullone	0.00524	3.18	0.192	1323	
133	FRAX486	0.000833	3.16	0.0736	700	
134	Brigatinib	0.00919	3.11	0.246	3312	X
135	SCH-28080	0.0000782	3.11	0.0134	3141	X
136	SB-268262	0.0114	3.1	0.271	1161	
137	METAPROTERENOL	0.00422	3.1	0.172	1089	
138	Fluocinonide (Vanos)	0.0113	3.09	0.271	1244	
139	PYR-41	0.00836	3.07	0.238	1725	
140	EC-144	0.00856	3.07	0.238	540	
141	Fedratinib (SAR302503. TG101348)	0.0148	3.06	0.308	1897	
142	piclamilast	0.00325	3.03	0.15	560	
143	R112	0.00401	3.01	0.169	2419	X
144	I-BET-762	0.0635	3	0.572	366	
145	2-cyanopyrimidine	0.00802	3	0.234	2758	X

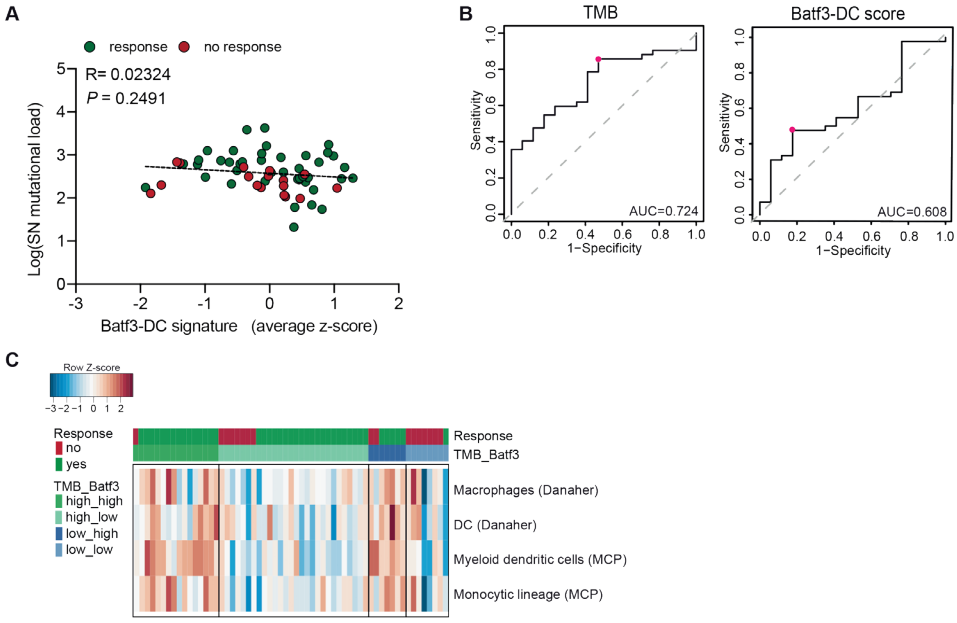

Figure S1 | Baseline Batf3 DC-score and TMB at baseline are not correlated. (A-B) RNA sequencing and whole exome sequencing of pre-treatment lymph node tumor biopsies of the OpACIN-neo study (neoadjuvant treatment ipilimumab + nivolumab, different dosing), including 59 patients for whom baseline tumor RNA sequencing and whole-exome sequencing data was available. **(A)** Correlation between Batf3-DC score and tumor mutational burden (TMB; plotted in log-scale) for patients with a response (green dots) or without a response (red dots). The correlation coefficient and *P* value were computed using the Pearson correlation method. **(B)** Summary receiver operating characteristic (sROC) curves for defining the optimal cut-off (marked by the red dot) of TMB (left) and Batf3 DC-score (right). The area under the sROC curve (AUC) for TMB was 0.724; optimal cut-off was 212. The AUC for Batf3-DC score was 0.608; optimal cut-off was 0.3756. **(C)** Patients of OpACIN-neo study for whom baseline tumor RNA sequencing and whole-exome sequencing data was available (n=59). Heatmap of RNA expression of macrophages and DC (based on Danaher immune cell signature) and myeloid dendritic cells and monocytic lineage (based on MCP counter) at baseline of patients ranked according to TMB and Batf3-DC score. Each column represents one patient (green: response; red: no response) and rows display immune subset.

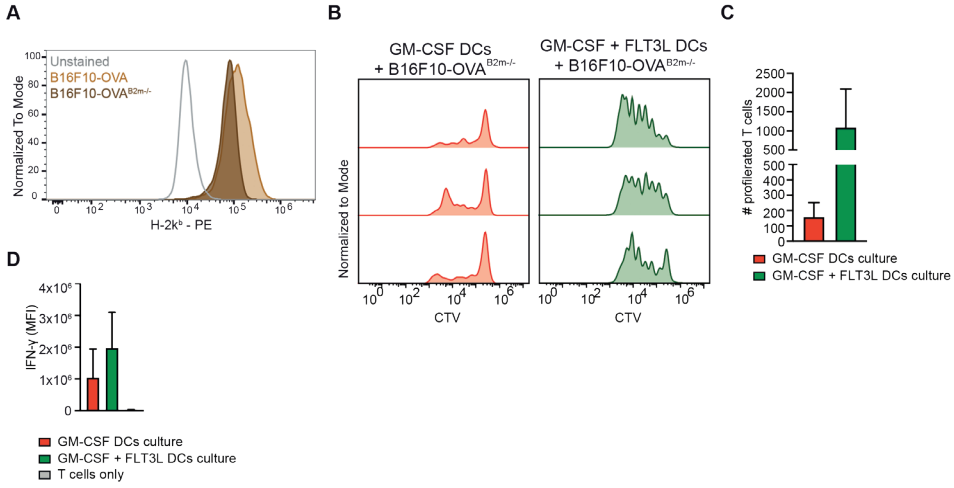

Figure S2 | Optimization cross-presentation assay for compound screen. (A) Flow cytometry plot for H-2k^{b} expression (as measure for MHC class I) for unstained cells (grey), B16F10-OVA cells (light brown) and B16F10-OVA$^{B2m-/-}$ cells (dark brown) after stimulation with IFN-γ. **(B-C)** Cross-presentation assay, loading GM-CSF DCs (red) or GM-CSF + FLT3L DCs (green) with irradiated (100Gy) B16F10-OVA$^{B2m-/-}$ cells with the addition of CpG ODN class B (1 μM), CTV-labelled OT-I TCR specific CD8^{+} T cells (10,000 cells each, 1:1:1). CD8^{+} T cells proliferation was assessed by flow cytometry (iQue Screener) after 4 days. **(B)** Representative histograms and **(C)** number of proliferated cells (measured by number of viable CTV-diluted CD8^{+} T cells, showing mean with SD). **(D)** IFN-γ secretion in the supernatant, measured by CBA after cross-presentation as described in (B), using GM-CSF DCs (red), GM-CSF + FLT3L DCs (green) or T cells only (grey) (showing mean with SD).

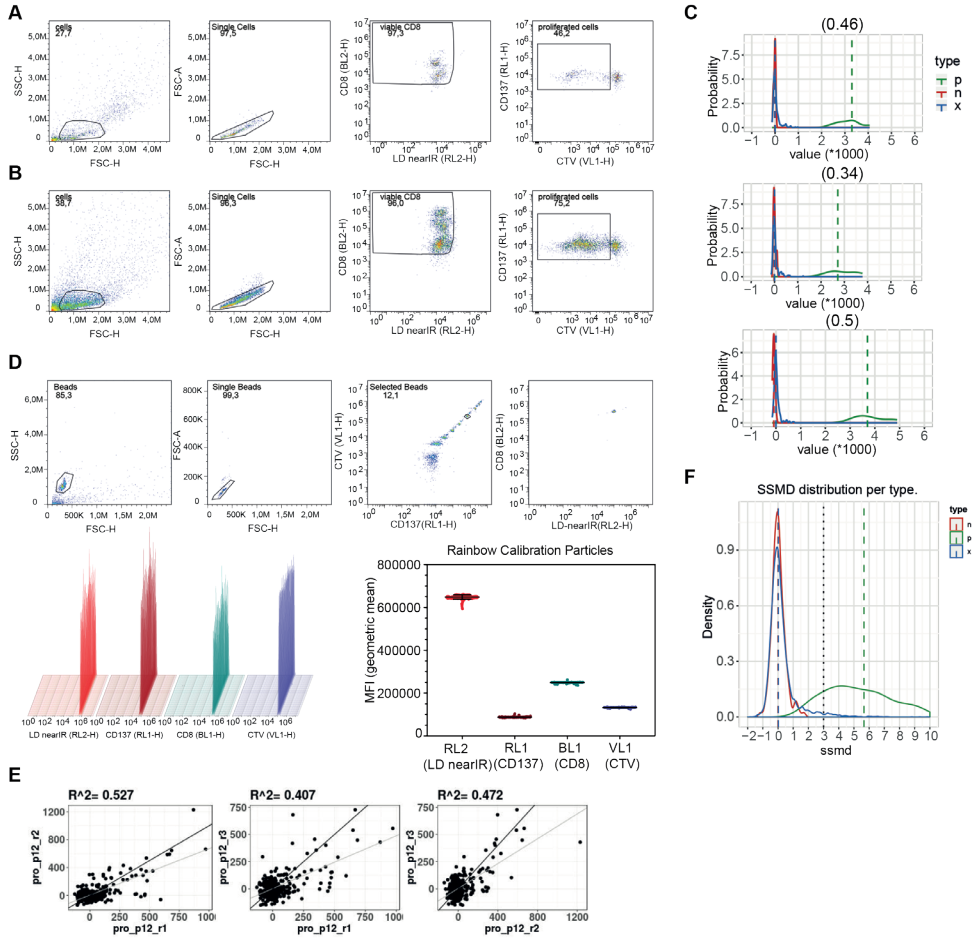

Figure S3 | Quality control of compound screen. (A-B) Flow cytometry analysis of compound screen. Gating strategy used for all wells, showing **(A)** negative control (GM-CSF DCs, B16F10-OVA$^{B2m-/-}$, CD8$^+$ T cells) and **(B)** positive control (GM-CSF + FLT3L DCs, B16F10-OVA$^{B2m-/-}$, CD8$^+$ T cells). Single cells were gated for viable CD8$^+$ T cells, and number of proliferated cells were determined by CTV dilution. **(C)** The Z-factor(43) was used to assess separation between normalized values of positive and negative control. Representative plots of one plate (for the 3 different replicates) are shown, in which the blue line represents the experiment wells, the red line represents the negative control, and green line the positive control. **(D)** Rainbow Calibration Particles (8 peaks) for the different lasers used in the screen (RL1, RL2, BL2, VL1) to assess performance of flow cytometer (iQue Screener). Each plate (n=21) contained 3 wells with Rainbow Calibration Particles. Representative gating strategy (upper panel), overlay of different wells (n=63; lower left panel), and MFI (geometric mean) of all wells (lower right panel) are shown. **(E)** Replicate correlation plot including linear regression (black line) with corresponding R^2 correlation factor. The replicates (n=3) of one representative compound plate are shown. **(F)** The strictly standardized mean difference (SSMD)(44) was calculated, showing the distribution for the negative control wells (red line), positive control wells (green line) and experimental wells (blue line). Hits were selected using a SSMD cut-off of ^{3}3 (dotted line).

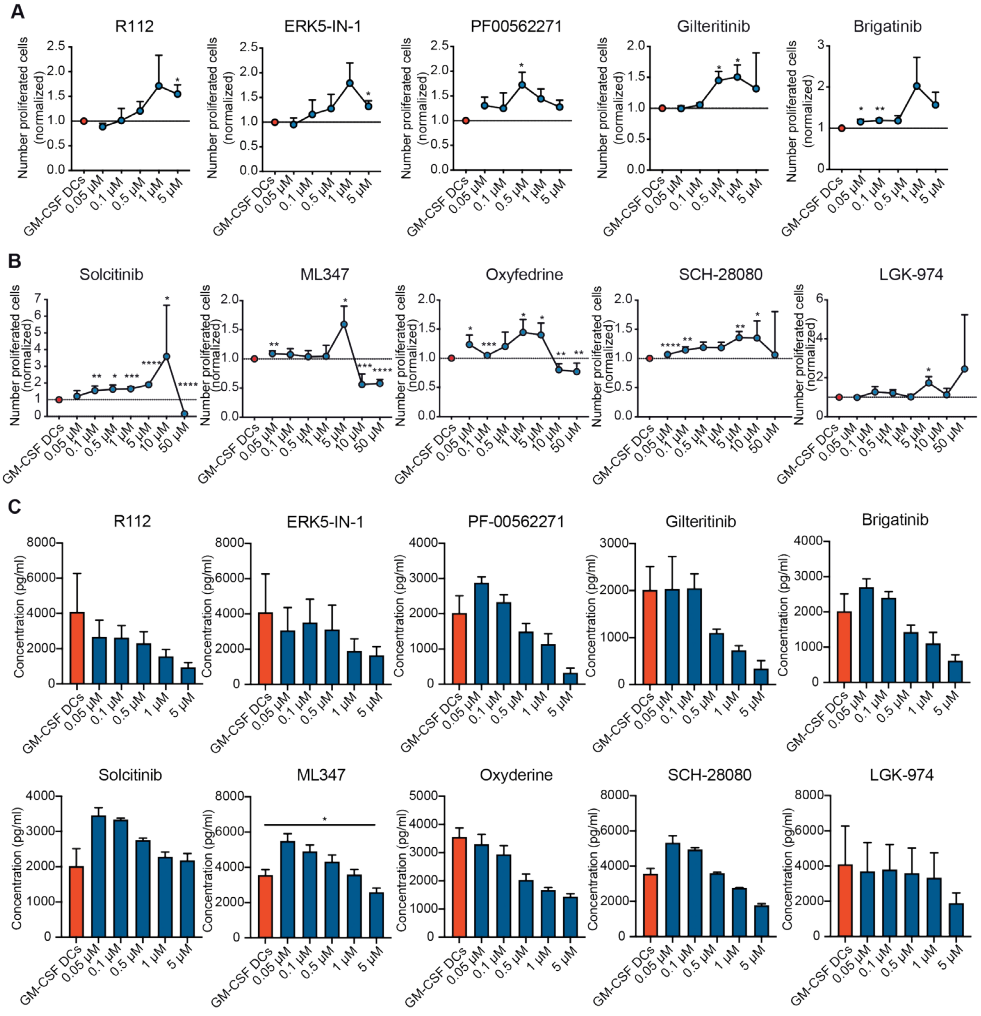

Figure S4 | Validation experiments using GM-CSF DCs in cross-presentation assay. (A-B) Validation experiments for the compounds where an effect was observed (11/20), repeating the same cross-presentation assay setting as in the screen, with the exception of using a dose range of **(A)** 0.05 µM – 5 µM and **(B)** 0.05 µM – 50 µM. The number of proliferated $CD8^+$ T cells was normalized to the proliferated $CD8^+$ T cells of DMSO control within an experiment (n=3-5 biological replicates, each with 3 technical replicates, showing mean with SEM). *P* value was calculated using an unpaired Student's t test, comparing the negative control (GM-CSF DCs, without drug but DMSO) and experimental well (dose of indicated compound). Significance is indicated above the dots. **(C)** TNF secretion in the supernatant, measured by CBA after cross-presentation as in (A-B) (showing mean with SEM). *P* value was calculated using an unpaired Student's t test, comparing the negative control (GM-CSF DCs, without drug but DMSO) and experimental well (dose of indicated compound). Significance is indicated above the dots. *, $P<0.05$, **, $P<0.01$, ***, $P<0.001$, ****, $P<0.0001$.

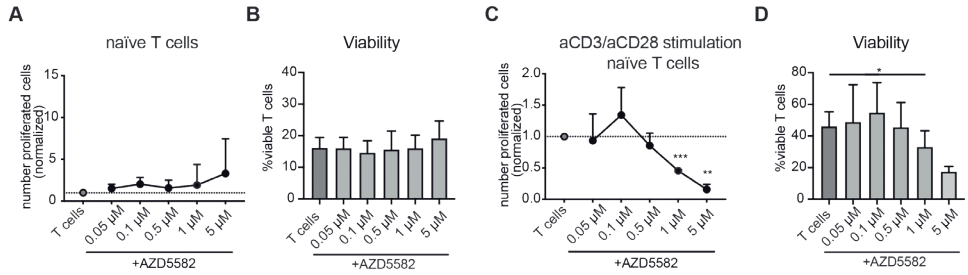

Figure S5 | Effect of AZD5582 on OT-I TCR specific CD8$^+$ T cells. (A) Effect of AZD5582 on naïve OT-I CD8$^+$ T cells. Naïve OT-I CD8$^+$ T cells were loaded with irradiated(100Gy) B16F10-OVA$^{B2m-/-}$ cells (10,000 each, 1:1) in the presence of DMSO (grey dot) or AZD5582 (0.05 µM – 5 µM; black dots) (n=4 biological replicates, each with 3-6 technical replicates, showing mean with SEM). The number of proliferated CD8$^+$ T cells was normalized to the proliferated CD8$^+$ T cells of DMSO control within an experiment. *P* value was calculated using an unpaired Student's t test, comparing the negative control (GM-CSF DCs, without drug but DMSO) and experimental well (dose of AZD5582). **(B)** Viability (assessed by live-dead stain by flow cytometry) of CD8$^+$ T cells in experiment as described in (A) (n=3 biological replicates, each with 3 technical replicates, showing mean with SEM). Significance was assessed by a paired Student's t test between the negative control (DMSO) and AZD5582 treatment (for different dosing). **(C-D)** Same experiments as described in (A-B), with the addition of anti-CD3 and anti-CD28 antibodies, to activate T cells (n=2). Significance is indicated above the dots. *, *P*<0.05, **, *P* <0.01, ***, *P* <0.001.

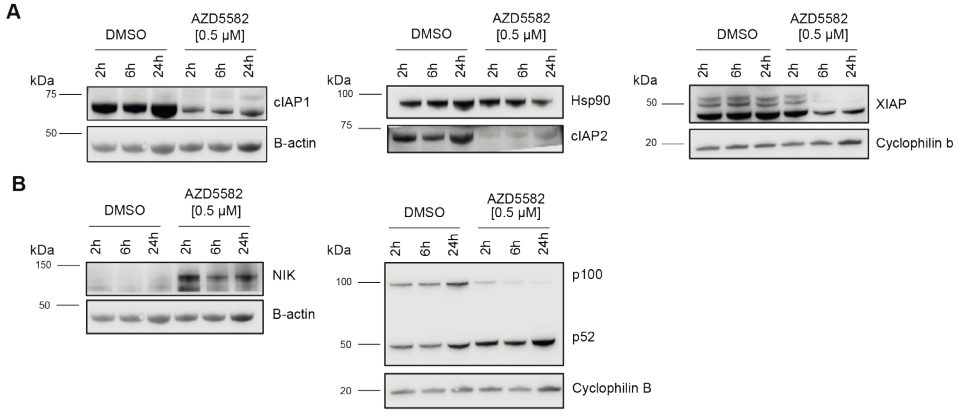

Figure S6 | Effect of AZD5582 on targets and downstream signaling in GM-CSF DCs. (A) The expression of cIAP1, cIAP2, XIAP and downstream signaling proteins of the non-canonical NF-kB pathway **(B)** NIK and **(C)** p52/p100 by GM-CSF DCs was assessed by western blot after AZD5582 treatment (0.5 µM or DMSO negative control) for 2, 6 or 24 hours. Cyclophilin b, β-actin or HSP90 was used as loading control.

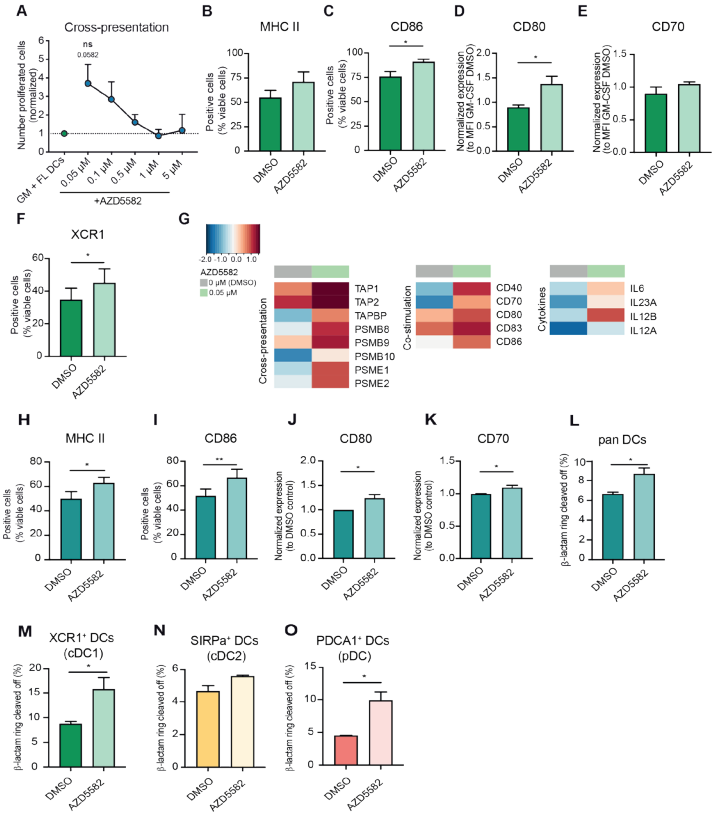

Figure S7 | Effect of AZD5582 on GM-CSF + FLT3L DCs and Pan-DCs. (A) Cross-presentation with GM-CSF + FLT3L DCs in the presence of AZD5582 (0.05 µM – 5 µM). Cross-presentation as in the screen, with exception of GM-CSF + FLT3L DCs instead of GM-CSF DCs. The negative control (GM-CSF + FLT3L DCs, without drug but DMSO) are displayed in green, and AZD5582 treatment in blue. T cell proliferation was normalized to the negative control. *P* value was calculated using unpaired Student's t test between DMSO and AZD5582 treatment (for different dosing) (n=3 biological replicates, each with 3 technical replicates, plotted as mean with SEM). **(B-F)** The expression of **(B)** MHC class II, **(C)** CD86, **(D)** CD80, **(E)** CD70 and **(F)** XCR1 on FLT3L + GM-CSF DCs assessed by flow cytometry after treatment with DMSO (dark green bar) or AZD5582 (0.05 µM; light green bar) after 24 hours. (B, C, F) Percentage of positive cells was determined and significance was assessed by a paired Student's t test between DMSO and AZD5582 treatment (n=3-4 biological replicates, each with 3 technical replicates, plotted as mean with SEM). (D-E) MFI was determined and within an experiment normalized to expression of DMSO treated GM-CSF DCs. An unpaired Student's t test between DMSO and AZD5582 was used to determine significance (n=3, biological replicates, each with 3 technical replicates, plotted as mean with SEM). **(G)** RNA sequencing of GM-CSF + FLT3L DCs treated with AZD5582 or DMSO control for 24 hours. Normalized average gene expression of indicated genes of three biological replicates were plotted in the heatmap. **(H-K)** Pan-DCs were isolated from spleens of Cas9-EGFP or WT C57BL/6JRj mice and cultured in the presence of DMSO (dark blue bar) or AZD5582 (0.5 µM; light blue bar) for 24 hours. Expression of **(H)** MHC class II, **(I)** CD86, **(J)** CD80 and **(K)** CD70 on Pan-DCs assessed by flow cytometry. (H-I) Percentage of positive cells was determined and significance was assessed by a paired Student's t test between DMSO and AZD5582 treatment (n=4 biological replicates, each with 2-3 technical replicates, plotted as mean with SEM). (J-K) MFI was determined and within an experiment normalized to DMSO control expression. An unpaired Student's t test between DMSO and AZD5582 was used to determine significance (n=4 biological replicates, each with 2-3 technical replicates, plotted as mean with SEM). **(L-O)** β-lactamase assay to monitor efficiency of antigen import into the cytosol for Pan-DCs treated with DMSO (dark bars) or 0.5 µM AZD5582 (light bars) for 24 hours (n=3). The percentage of cleaved off CCF4 in the cells was measured using flow cytometry for **(L)** all isolated Pan-DCs, **(M)** $XCR1^+$ cells of the Pan-DC, **(N)** $SIRPa^+$ cells of the Pan-DCs, **(M)** $PDACA1^+$ cells of the Pan-DCs. P value was calculated using an unpaired t test. *, $P<0.05$, **, $P<0.01$

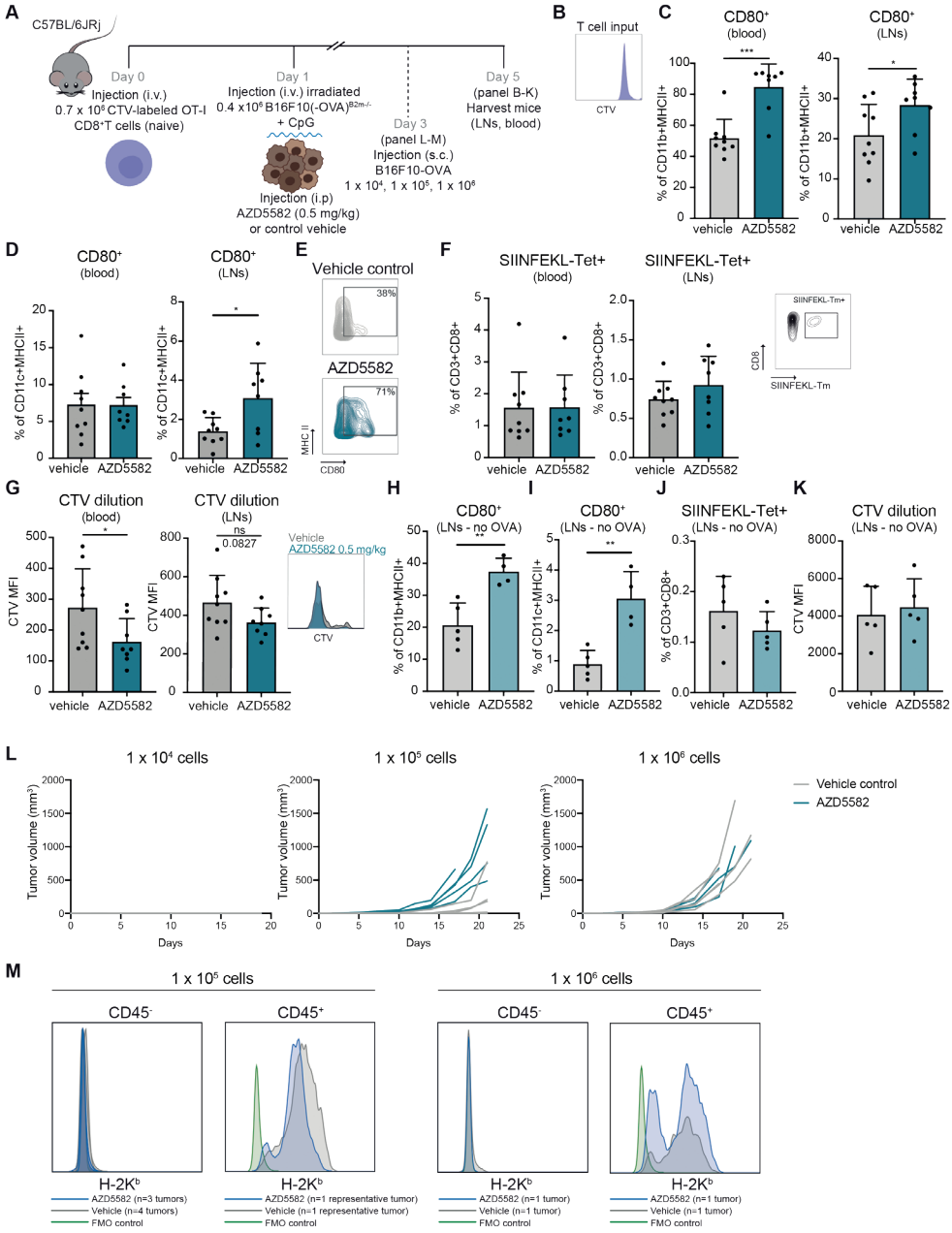
A
C57BL/6JRj
Day 0
Injection (i.v.)
0.7 x 10⁶ CTV-labeled OT-I CD8⁺T cells (naive)
Day 1
Injection (i.v.) irradiated
0.4 x10⁶ B16F10(-OVA)B2m-/-
+ CpG
Injection (i.p)
AZD5582 (0.5 mg/kg)
or control vehicle
Day 3
(panel L-M)
Injection (s.c.)
B16F10-OVA
1 x 10⁴, 1 x 10⁵, 1 x 10⁶
Day 5
(panel B-K)
Harvest mice
(LNs, blood)
B
T cell input
CTV
C
CD80⁺ (blood)
CD80⁺ (LNs)
% of CD11b+MHCII+
vehicle
AZD5582
D
CD80⁺ (blood)
CD80⁺ (LNs)
% of CD11c+MHCII+
E
Vehicle control
AZD5582
38%
71%
MHC II
CD80
F
SIINFEKL-Tet+ (blood)
SIINFEKL-Tet+ (LNs)
% of CD3+CD8+
SIINFEKL-Tm+
CD8
SIINFEKL-Tm
G
CTV dilution (blood)
CTV dilution (LNs)
CTV MFI
ns
0.0827
Vehicle
AZD5582 0.5 mg/kg
CTV
H
CD80⁺ (LNs - no OVA)
I
CD80⁺ (LNs - no OVA)
% of CD11c+MHCII+
J
SIINFEKL-Tet+ (LNs - no OVA)
% of CD3+CD8+
K
CTV dilution (LNs - no OVA)
CTV MFI
L
1 x 10⁴ cells
1 x 10⁵ cells
1 x 10⁶ cells
Tumor volume (mm³)
Days
Vehicle control
AZD5582
M
1 x 10⁵ cells
1 x 10⁶ cells
CD45⁻
CD45⁺
H-2Kᵇ
AZD5582 (n=3 tumors)
Vehicle (n=4 tumors)
FMO control
AZD5582 (n=1 representative tumor)
Vehicle (n=1 representative tumor)
AZD5582 (n=1 tumor)
Vehicle (n=1 tumor)

Figure S8 | *in vivo* vaccination model testing AZD5582. (A) Naïve CTV-labeled OT-I TCR specific $CD8^+$ T cells were injected (0.7 x 10^6, i.v.) in C57BL/6JRj recipient mice. After one day, irradiated (100Gy) B16F10-$OVA^{B2m-/-}$ or $B16F10^{B2m-/-}$ + CpG ODN class B were injected (0.4 x 10^6 cells, i.v.) and AZD5582 (0.5 mg/kg) or vehicle control was injected (i.p.). On day 5, lymph nodes and blood were harvested (panel B-K). For panel L-M, mice were injected (s.c.) with B16F10-OVA cells (10,000, 100,000 or 1,000,000) on day 3. **(B)** Flow cytometry analysis of CTV labeling on $CD3^+CD8^+$ OT-I T cells. **(C-E)** $CD80^+$ expression on **(C)** $CD11b^+$MHC class II^+ cells and **(D)** $CD11c^+$MHC class II^+ cells in the blood and lymph nodes of mice that were injected with B16F10-$OVA^{B2m-/-}$ and treated with vehicle control (grey; n=9) or AZD5582 (blue; n=8). Error bars indicate SD. Significant difference was assessed by an unpaired Student's t test. **(E)** Representative flow cytometry analysis. **(F-G)** Flow cytometry analysis of **(F)** percentage SIINFEKL-$Tetramer^+$ cells of $CD3^+CD8^+$ cells **(G)** MFI of CTV of SIINFEKL-$Tetramer^+CD3^+CD8^+$ cells in the blood and lymph nodes of mice that were injected with B16F10-$OVA^{B2m-/-}$ and treated with vehicle control (grey; n=9) or AZD5582 (blue; n=8). Error bars indicate SD. Significant difference was assessed by an unpaired Student's t test. **(H-I)** $CD80^+$ expression on **(H)** $CD11b^+$MHC class II^+ cells and **(I)** $CD11c^+$MHC class II^+ cells in the lymph nodes of mice that were injected with $B16F10^{B2m-/-}$ and treated with vehicle control (grey; n=5) or AZD5582 (blue; n=5). Significant difference was assessed by an unpaired Student's t test. Error bars indicate SD. **(J-K)** Flow cytometry analysis of **(J)** percentage SIINFEKL-$Tetramer^+$ cells of $CD3^+CD8^+$ cells **(K)** MFI of CTV of SIINFEKL-$Tetramer^+CD3^+CD8^+$ cells in the lymph nodes of mice that were injected with $B16F10^{B2m-/-}$ and treated with vehicle control (grey; n=5) or AZD5582 (blue; n=5). **(L)** Individual tumor growth curves of C57BL/6JRj mice injected with different amount of B16F10-OVA tumor cells on day 3 after vaccination. On day 1, mice received naïve CTV-labeled OT-I TCR specific $CD8^+$ T cells (1 x 10^6, i.v.). After one day, irradiated (100Gy) B16F10-$OVA^{B2m-/-}$ + CpG ODN class B were injected (0.4 x 10^6 cells, i.v.) and AZD5582 (0.5 mg/kg) or vehicle control was injected (i.p.). On day 3, mice were s.c. injected with either 10,000 (n=9), 100,000 (n=10) or 1,000,000 (n=9) B16F10-OVA tumor cells. Mice that received previous treatment with vehicle are displayed in grey and mice received previous treatment with AZD5582 are displayed in blue. **(M)** Flow cytometry analysis of tumors of mice on day 24 after s.c. B16F10-OVA tumor inoculation. The expression of H-$2K^b$ expression for the $CD45^-$ and $CD45^+$ population is shown, including a fluorescence minus one control (FMO). *P* value is indicated above the bars or between groups. Error bars indicate SD. *, $P<0.05$, **, $P<0.01$, ***, $P<0.001$

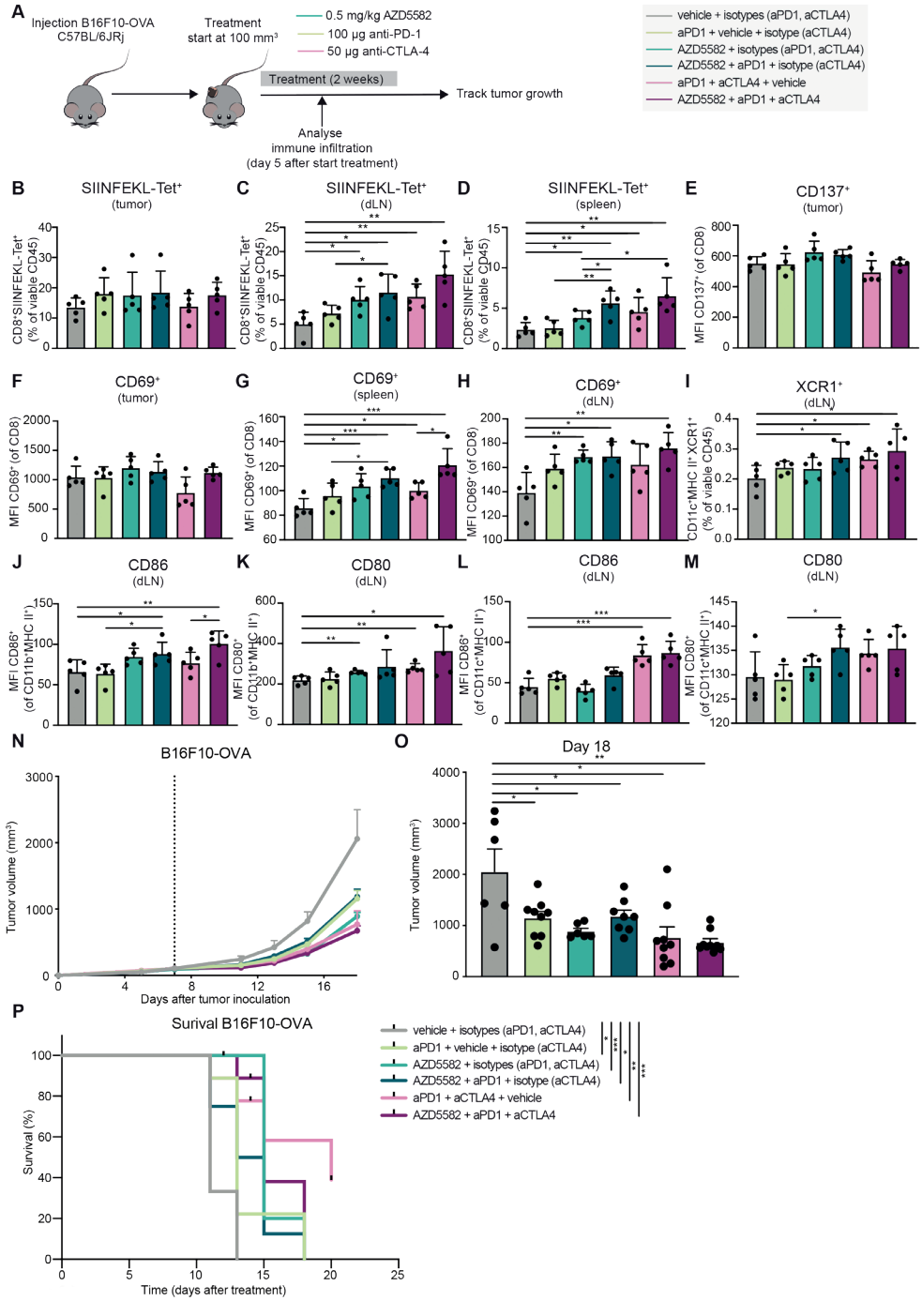
A
Injection B16F10-OVA C57BL/6JRj
Treatment start at 100 mm³
0.5 mg/kg AZD5582
100 µg anti-PD-1
50 µg anti-CTLA-4
Treatment (2 weeks)
Track tumor growth
Analyse immune infiltration (day 5 after start treatment)
vehicle + isotypes (aPD1, aCTLA4)
aPD1 + vehicle + isotype (aCTLA4)
AZD5582 + isotypes (aPD1, aCTLA4)
AZD5582 + aPD1 + isotype (aCTLA4)
aPD1 + aCTLA4 + vehicle
AZD5582 + aPD1 + aCTLA4
B SIINFEKL-Tet+ (tumor)
C SIINFEKL-Tet+ (dLN)
D SIINFEKL-Tet+ (spleen)
E CD137+ (tumor)
F CD69+ (tumor)
G CD69+ (spleen)
H CD69+ (dLN)
I XCR1+ (dLN)
J CD86 (dLN)
K CD80 (dLN)
L CD86 (dLN)
M CD80 (dLN)
N B16F10-OVA
Tumor volume (mm³)
Days after tumor inoculation
O Day 18
P Surival B16F10-OVA
Survival (%)
Time (days after treatment)

Figure S9 | AZD5582 treatment of B16F10-OVA tumor bearing mice. (A) C57BL/6JRj mice were injected with B16F10-OVA cells (0.5 x 10^6, s.c. on the right flanks) and treatment with vehicle + isotype controls (for anti-PD-1, anti-CTLA-4), anti-PD-1 + vehicle control + isotype control (anti-CTLA-4), AZD5582 + isotype controls (for anti-PD-1, anti-CTLA-4), anti-PD-1 + AZD5582 + isotype control (anti-CTLA-4), anti-PD-1 + anti-CTLA-4 + vehicle or anti-PD-1 + anti-CTLA-4 + AZD5582 was given i.p. for two weeks. On day 5 after treatment start, tumors, lymph nodes, and spleens were harvested from satellite mice and analyzed by flow cytometry. Tumor growth of all other mice was monitored. **(B-D)** Flow cytometry analysis of percentage $CD8^+$SIINFEKL-Tetramer$^+$ cells of viable CD45 cells in **(B)** tumor (n=5), **(C)** lymph node (n=5), **(D)** spleen (n=5). **(E-H)** Flow cytometry analysis of $CD8^+$ cells for the expression of **(E)** CD137 in the tumor (n=5), **(F)** CD69 in the tumor (n=5), **(G)** CD137 in the spleen (n=5), **(H)** CD137 in the lymph node (n=5). **(I-M)** Flow cytometry analysis of the lymph node for **(I)** the percentage of $CD11c^+$MHC class II^+XCR1^+ of viable CD45 cells (n=5) and the expression of **(J)** CD86 on $CD11b^+$MHC class II^+ cells (n=5), **(K)** CD80 on $CD11b^+$MHC class II^+ cells (n=5), **(L)** CD86 on $CD11c^+$MHC class II^+ cells (n=5) and **(M)** CD80 on $CD11c^+$MHC class II^+ cells (n=5). *P* value was calculated using unpaired Student's t test comparing the different treatment groups. **(N)** Average tumor size of the treatment groups, the start of treatment (day 7) is indicated with a dotted line (showing mean with SEM). **())** Tumor volume on day 18, showing mean with SEM. An unpaired Student's t test comparing the different treatment groups was used to determine significance. **(P)** Kaplan-Meier survival curve of all mice. Statistical testing was performed by Long-rank test. *P* value is indicated above the bars. *, $P<0.05$, **, $P<0.01$, ***, $P<0.001$.